Investigation of Hydrodynamics at the Wall and in the Bulk With RICM

by

Sebastian Diego Walter Thomas

Bachelor thesis in physics
presented to the faculty of physics, mathematics and informatics (FB 08)
of Johannes Gutenberg University Mainz
on 22nd of June 2015

1st corrector: Prof. Dr. Thomas Palberg
2nd corrector: Prof. Dr. Hans-Jürgen Butt

I hereby declare that this dissertation has been composed by me. All information, statements and research data were established by me, if not referenced to someone else. This thesis has not been presented for any kind of award before. References to previous papers and research results are provided and accurate.

Mainz, 22th of June 2015

Sebastian Diego Walter Thomas
AK Butt
Max Planck Institute for Polymer Research
Ackermannweg 10
D-55128 Mainz
thomas@mpip-mainz.mpg.de

Abstract

Untersuchung von Hydrodynamik an Grenzflächen und Fern von Grenzflächen mit Hilfe von Interfereometrie

Die vorliegende Bachelorarbeit wurde am Max-Planck-Institut für Polymerforschung erstellt und beschäftigt sich mit der Messungen der Hydrodynamik auf mikroskopischer Skala. Mithilfe einer optischen Falle und eines Interfereometers wurde eines der kleinsten Kugelfallviskosimeter der Welt realisiert. Das Viskosimeter erlaubt Messungen an mikrometer großen Kugeln in einer Vielzahl von optischen Flüssigkeitszellen.
In dieser Arbeit konnte ich zeigen, dass es möglich ist mithilfe dieser Apparatur durch freie Sedimentation von Mikrokügelchen aus Glas deren Materialeigenschaften, wie z.B. Radius oder Dichte, akurat zu bestimmen sowie die Tatsache, dass sämtliche Messungen an ihr reproduzierbar sind. Ebenso kann bei bekannten Kugeleigenschaften die Viskosität der umgebenden Flüssigkeit bestimmt werden. Ein weiterer Fokus dieser Arbeit lag auf der Untersuchung von Wandeffekten, die die Sedimentation in der Nähe einer Wand beeinflussen. Unter Berücksichtigung solcher Wandeffekte konnte ich zeigen, dass Messungen, bei denen eine Kugel nahe einer Wand sedimentierte zu äquivalenten Ergebnissen führten wie Messungen, bei denen eine Kugel fern einer Wand frei sedimentieren konnte.

The present bachelor thesis was written at the Max Planck Institute for Polymer Research and addresses the measuring of hydrodynamics on a microscopic scale. The combination of an optical trap and an interferometer forms one of the smallest falling sphere viscosimeters of the world. This viscosimeter enables measurements with spheres with radii in the range of micrometers in optical fluid cells.
With this work I was able to show that it is possible to determine properties of small glass spheres, like the radius or the density, by sedimentation experiments as well as the fact that all measurements are reproducible. Furthermore this work was focussed on the examination of wall effects, which influence sedimentations near walls. Considering these wall effects I was able to show, that measurements of sedimentations of a sphere beginning at the wall yield equivalent outcomes to a sedimentation far away from a wall.

Contents

1. Introduction

In every situation where movement in a fluid is involved hydrodynamic forces will arise and influence the trajectories of particles or the fluid itself. Thus, accurate knowledge of those forces is crucial for many scientific and industrial areas of application. For example the field of interface and colloid science addresses research on microscopic small particles dispersed in certain media such as fluids in order to enable technological advance in pharmaceuticals, biotechnologies and many more. An example for an industry which uses knowledge about hydrodynamic forces on a much larger scale could obviously be shipbuilding.
A step towards better knowledge about these fundamental forces is the combination of hydrodynamical research and optical trapping. It opens the possibility to examine the interaction of particles dispersed in fluids on a microscopic level with a resolution of a few nanometres. The Department Butt at the Max Planck Institute for Polymer Research in Mainz is concerned with scientific research on the physics of interfaces and thus uses this combination of techniques to survey the behaviour of microspheres near interfaces like a wall of a glass sample cell.
Definite measurements are enabled by another technique, named Reflection Interference Contrast Microscopy. RICM allows us to exactly survey the movement of a colloid in the sample cell over comparable long distances.
Such an optical trap was constructed by Dominik Pilat at the MPIP in the Department Butt. While it is the declared goal to perform experiments in high pressure cells with it, it is important to get to know the specific characteristics of measurements and the nature of hydrodynamics in such small dimensions. I was offered the opportunity to perform my bachelor thesis at the optical trap and do research on hydrodynamics with it.
My work is focussed on the free sedimentation of spheres of fused silica with diameters between five and eight micrometres unter amospheric pressure. In my experiments I will determine the viscosities for different fluids, i.e. water and aqueous glycerol solutions, with different microspheres. Thus, the combination of RICM and a small sample cell in the optical trap resembles one of the smallest falling sphere viscosimeters of the world. Since the goal is to measure forces at the wall of the samples I will not restrict the sedimentations to the bulk in the middle of the sample cell, but I will measure sedimentations beginning directly at the wall of the glass cell, too.
The goal of my bachelor thesis is to measure viscosities as well as preparing further experiments on this optical trap. I will examine which microspheres are to use in order to get reliable data from the measurements and which experiments are necessary to give the scientist all the data needed to effectively and decently evaluate his or her work.

2. Theory

In this first part I will briefly discuss all the physical principles that are vital for the understanding of the performed experiments and their analysis.

2.1. Hydrodynamic Forces

2.1.1. Viscosity

For all hydrodynamic forces the viscosity plays an important role. It is an indicator for the reluctance of a fluid against forming velocity gradients in itself. A more unscientific term would be thickness.

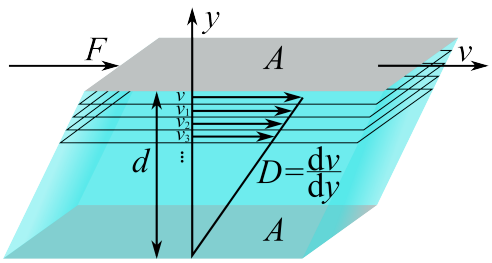

Figure 2.1.: Two plates with surface A, distance d and a certain fluid between them are moved against each other with the force F and velocity v. Because the neighbouring layers move with each plate a velocity gradient D is established.
Source: `http://upload.wikimedia.org/wikipedia/commons/9/9a/Definition\_Viskositaet.png`,
(25^{th} of May, 2015).

For the definition of Viscosity see figure 2.1.1. The force F needed to move the upper plate is proportional to the surface $F \propto A$ and the velocity gradient $F \propto \frac{dv}{dy}$ and thus we get the equation

$$F = \eta A \frac{dv}{dy} \tag{2.1}$$

with the viscosity η as the constant of proportionality [10]. Its unit is $[\eta] = mPa \cdot s$. The viscosity is exponentially dependent on the temperature of the fluid, higher temperature leads to lower viscosity and vice versa. For water the viscosity at 20 degrees

Celsius is $\eta_{H_2O,\ 20°C} = 1.002\ mPa \cdot s$ [16] and for glycerol $\eta_{glyc,\ 20°C} = 1480\ mPa \cdot s$ [5].
Cheng published 2008 a formula which allows to calculate the viscosity of aqueous glycerol solutions with an arbitrary mixing ratio for temperatures ranging from zero to hundred degrees Celsius [6]. On the internet presence [4] an implementation can be found, which calculates for a given ratio of mixture and temperature the viscosity with Cheng's formula.

2.1.2. Flow

When a particle, for example a small sphere like in my work, flows in a fluid, it will always experience a drag opposed to the direction of movement. This force is caused by dynamic friction with the molecules of the medium and increases with the velocity of the particle, its radius and the viscosity of the fluid.

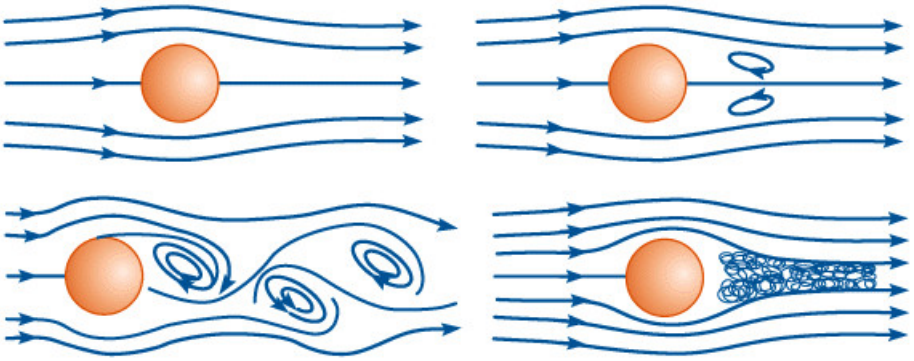

Figure 2.2.: On the first (upper left) picture laminar flow is illustrated and on the last (lower right) one turbulent flow with small eddies and vortices. The second and third graphics show possible transitions between both states. Source: `https://elearning.physik.uni-frankfurt.de/data/FB13-PhysikOnline/lm\_data/lm\_324/daten/bild\_3/06\_0570.gif`,
(25^{th} of May, 2015)

It is essential for the calculations of hydrodynamic forces to determine whether the movement of the spheres causes laminar or turbulent flow, see figure 2.1.2. Therefore one can form the ratio of inertial and frictional forces, known as the *Reynolds Number*

$$Re = \frac{\text{inertial forces}}{\text{frictional forces}} = \frac{\frac{\rho \vec{v}^2}{L}}{\frac{\eta \vec{v}}{L^2}} = \frac{\rho \vec{v} L}{\eta} \tag{2.2}$$

with η: the dynamic viscosity of the medium,
$\vec{v}_s$:the velocity of the sphere,

ρ: the density of the medium,
L: the characteristic length of the system, in this case given by the diameter of a sphere R_s.

A large Reynolds Number $Re \gg 1$ indicates to the existence of turbulences and flow instabilities in general, whereas for a small Reynolds Number $Re \ll 1$ laminar flow can be assumed.
In the second case the hydrodynamic drag force (and therefore the movement of the particle) can be well described by *Stoke's Law*, which reads

$$\vec{F}_{fr} = -6\pi\eta r_s \vec{v}_s. \tag{2.3}$$

Turbulent flow is, due to vortices and eddies, more or less unpredictable and hence not as easy to calculate.
For each of my experiments laminar flow was dominant and therefore all calculations can be based upon Stoke's Law.

2.1.3. Hydrodynamic interaction near a wall

Here I will largely follow the explanations of Butt and Kappl [3].
Near walls the hydrodynamic drag will increase due to fluid that has to be removed from between the sphere and the wall, when approaching the plane. When diverging from the wall, the fluid has to fill the gap and so the same force in the opposite direction arises.
Therefore the equation 2.3 has to be modified. Without loss of generality we can consider the velocity of the sphere $\vec{v}_s$ to be perpendicular to the plane and will therefore be written as $\vec{v}_{s\perp}$. Brenner introduced 1961 an equation of the following form:

$$F_{fr} = -6\pi\eta\vec{v}_{s\perp} r_s \lambda_B \tag{2.4}$$

with the factor λ_B, which I will call the Brenner factor in my thesis. It reads as following:

$$\lambda_B = \frac{4}{3} sinh(\beta) \sum_{n=1}^{\infty} \left(\frac{n(n+1)}{(2n-1)(2n+3)} \left(\frac{2sinh((2n+1)\beta) + (2n+1)sinh(2\beta)}{4sinh^2((n+0,5)\beta) - (2n+1)^2 sinh^2(\beta)} - 1 \right) \right) . \tag{2.5}$$

with $\beta = \frac{1}{cosh(\frac{D+r_s}{r_s})}$,
and D: the distance between surface and sphere.
Butt and Kappl suggest an approximated version for the Brenner factor

$$\lambda_B = 1 + \frac{r_s}{D} , \tag{2.6}$$

which leads to

$$F_{fr} = -6\pi\eta\vec{v}_{s\perp} r_s \left(1 + \frac{r_s}{D}\right) . \tag{2.7}$$

One can easily see that for distances much grater than the radius of the particle $D \gg R_s$ the equation resembles the original expression by STOKES, whilst for small distances $D \ll R_s$ the dragging force will increase up to infinity. That clearly opposes what we can examine in a lab, because it is possible to bring a sphere in contact with a plane. The cause for this discrepancy lies in the implicit use of the fluid approximation, which describes the particles in the fluid as in thermodynamic equilibrium and thus they are treated as a fluid. But on a molecular scale where quantum dynamics start to play a role, this approximation is no longer suitable.
For fitting the sedimentations at the wall with equation 2.7 I substitute $v_s = \frac{dD}{dt}$, since these are the measured parameters. It yields

$$F = -6\pi\eta r_s(1 + \frac{r_s}{D})\frac{dD}{dt} \ .$$

Integration and reorganization yields

$$t = -\alpha r_s(D - D_0) - \alpha r_s^2 ln(D - D_0) + t_0 \ , \tag{2.8}$$

with $\alpha = \frac{6\pi\eta}{F}$.

2.2. The Basics of Gaussian Beams

To understand the working principles of an optical trap it is indispensable to have basic knowledge about Gaussian beams available. For that reason this chapter exists and will focus on the most important facts to understand my work. The information presented is taken from [8].
Whilst there are lot of different modes in which a laser resonator can operate I will only focus on the best known, the Gaussian beam or TEM_{00} mode, because its the one mostly used for trapping particles.
The Gaussian beam earns his name from its intensity profile which can be well approximated by a Gaussian function. The advantage in using the TEM_{00} mode lies in its feature that a refracted beam (e.g. by a lens) is always a Gaussian beam, too.
To talk about the characteristics of a Gaussian beam we have to define a beam radius, because clearly a laser beam doesn't provide a definite edge. Therefore we define that the beam radius is the position, where the intensity has fallen to $\frac{1}{e^2}$ or $13,5$ %. Another possible definition would have been at FWHM.
A laser beam will be narrowest at a certain position (i.e. the focus of the beam), which is called the beam waist, and with further propagation it will widen up, but not linearly, see also figure 2.3.
To describe the propagation of such a beam only a few parameters are sufficient. The first piece of information one needs is the wavelength λ. The second value needed is the beam radius at the position of the beam waist ω_0. These two parameters allow us to determine all important aspects of the spreading of the laser beam.
The $\frac{1}{e^2}$ radius of the beam can be calculated using the following equation

$$\omega(z) = \omega_0\sqrt{1 + \left(\frac{\lambda z}{\pi\omega_0^2}\right)^2}. \tag{2.9}$$

The opening of the beam, defined by the angle θ, will approach this asymptotically

$$\theta = \frac{\lambda}{\pi\omega_0} \tag{2.10}$$

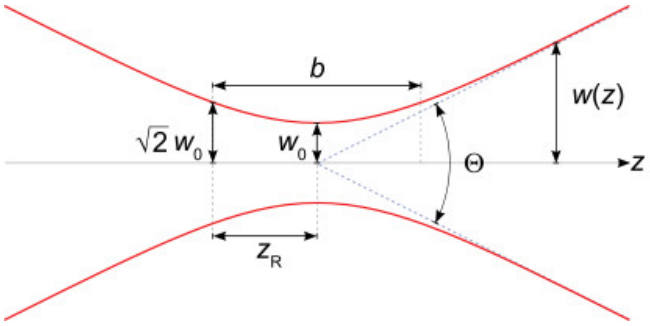

Figure 2.3.: In this figure is the propagation of a Gaussian along the z axis shown. $\omega(z)$ is the beam radius at position z, ω_0 is the radius at the beam waist, Z_R is the Rayleigh length, θ is the opening of the beam for large z. Source: `http://upload.wikimedia.org/wikipedia/commons/thumb/5/53/GaussianBeamWaist.svg/416px-GaussianBeamWaist.svg.png`

for a large value of z. This equation is based on the small angle approximation $sin(\theta) = \theta$. One last important magnitude is the Rayleigh length, at which the beam will be widened by a factor of $\sqrt{2}$. It can be calculated by the equation

$$Z_R = \frac{\pi\omega_0^2}{\lambda}. \tag{2.11}$$

2.3. Optical Trapping

In optical trapping one uses the Gaussian intensity distribution of the laser beam to trap a particle in the lateral dimensions. This was introduced in the 1970s by Ashkin [1]. Two equivalent explanations exist.
The microspheres are made of dielectric material, such as glass or polymers. Near a laser beam, that means near a strong electro magnetic field, they form electric dipoles and therefore are attracted by the area of the highest intensity of the electric field. That means the particle is dragged into the laser beam by the gradient force until it is trapped in its centre [13].
The other possible explanation uses the momentum of refracted photons of the laser beam. It is shown in figure 2.4. Because in the centre of the beam is the highest intensity there are the most photons. If a bead is shifted of the centre more photons will travel through it on the side nearer the centre and get refracted to the middle of the bead. The change of momentum of the photons yields a nett force to the centre of the beam [14].
This explanation makes it obvious that the particles, which shall be trapped, must have a higher refractive index than the surrounding medium. Otherwise they would be pushed out of the beam because the photons would be refracted out of the bead.
A very essential force is the radiation pressure of a beam on the trapped particle. This force is the reason why a bead gets pushed along the direction of the laser. It occurs due to backscattered and absorbed photons in the beam. The momentum of those photons (which is logically in direction of the laser beam) transfers to the bead and moves it [13].
By focussing the beam very sharply one can achieve trapping in the longitudinal dimension, too. Therefore you have to by overcome the radiation pressure, which then resembles an

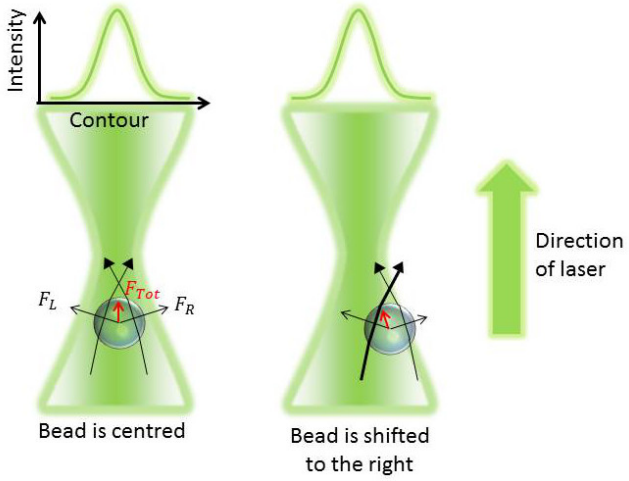

Figure 2.4.: The working principle of an optical trap with Gaussian beams. The right side shows the forces due to refraction of photons in equilibrium. On the left side one can see that the total force becomes shifted towards the centre of the beam, when the bead is not centred.

optical tweezers. However, this is not done in our trap and therefore I will not go into detail here. Nevertheless, strong focussing is needed in our system too.

2.4. RICM

Reflection Interference Contrast Microscopy is a technique that allows us to measure longitudinal movement in our sample, for example the sedimentation of particles. In this section I will follow the explanations of Limozin and Sengupta [12].
The basic idea of RICM is that, as the name suggests, reflected laser beams interfere with each other. Therefore a laser beam enters the sample and thus the first reflected beam (with intensity I_1) originates from the interface air/glass. The transmitted beam is again partly reflected at the interface medium/particle (intensity I_2), since the particle is trapped in the trapping laser beam, which is coaxial to the interference laser beam.
The reflected rays follow a certain beam path and are guided onto a diode to measure the intensity of their interference. This signal in the context of an additional time signal allows us to calculate the sedimentation velocity, since the intensity I is given by

$$I = I_1 + I_2 + 2\sqrt{I_1 I_2} cos(2kh) \ , \tag{2.12}$$

with h: distance between particle and air/glass interface,
k: wave vector $k = \frac{2\pi n_m}{\lambda}$ and
n_m: the refraction index of the surrounding medium.

Since we are only interested in the minima and maxima of the signal we shorten the above expression to

$$I \sim cos(\frac{4\pi h n_m}{\lambda}) \ ,$$

and then it is obvious that for an extrema the expression $\frac{4n_{medium}h}{\lambda}$ must be an integer. Therefore we can calculate the distance a particle travelled between to extrema of the interference with

$$h = \frac{\lambda}{4n_m} \ . \tag{2.13}$$

3. The Experiment and General Execution

In this chapter I will discuss the important parts of the optical trap and about the general execution of the experiments and evaluation of the collected data.
All trials were conducted in a precision cell made of quartz SUPRASIL ®, manufactured by Hellma Analytics (Type No. 110-QS), with a light path of $d = 1\ mm$. In figure 3.1 a simplified sketch shows the general implementation of a sedimentation experiment, where a microsphere is pushed with the green trapping laser to the upper wall of the cell while the movement can be measured with help of the red laser by RICM.

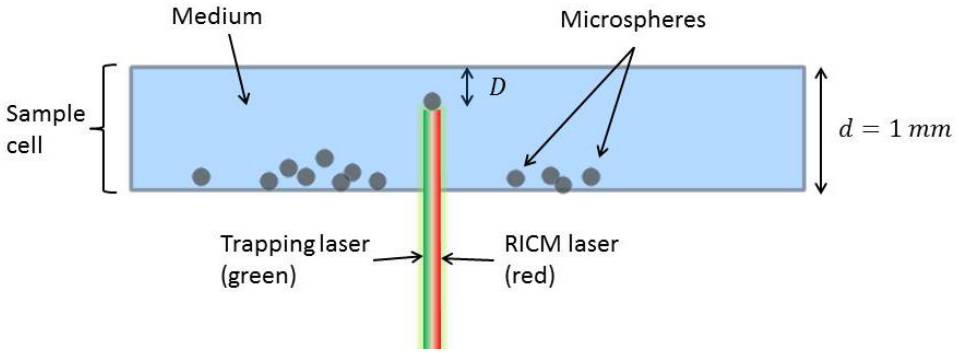

Figure 3.1.: Simplified description, which is not in scale, of the proceedings in the sample cell. The green laser pushes a bead to the upper wall of the cell, while the red laser (which is exactly coaxial with the green one) allows to measure the movement via RICM. The distance from the lower to the upper wall is $d = 1\ mm$.

To perform my measurements, I needed the setup described in the following section.

3.1. The Components of the Optical Trap

An schematic overview over the important parts of the setup can be seen in figure 3.2. In this section I will explain all parts, that are shown in the graphic.
The centrepieces of the optical trap are the two lasers:

- The high power trapping laser is made by Laser Quantum and from the type Finesse pure (FPU60). That is a Nd:YAG laser with a wavelength of 532 nm and therefore is seen as green light. The power can be raised up to four Watt, but was mostly operated around three Watt and was attenuated to less than one Watt. This was done because a laser runs more stable when operating at the upper part of its power range. Its beam gets split up and both parts follow their paths to the sample cell, one enters from above and the other one from under the sample stage.

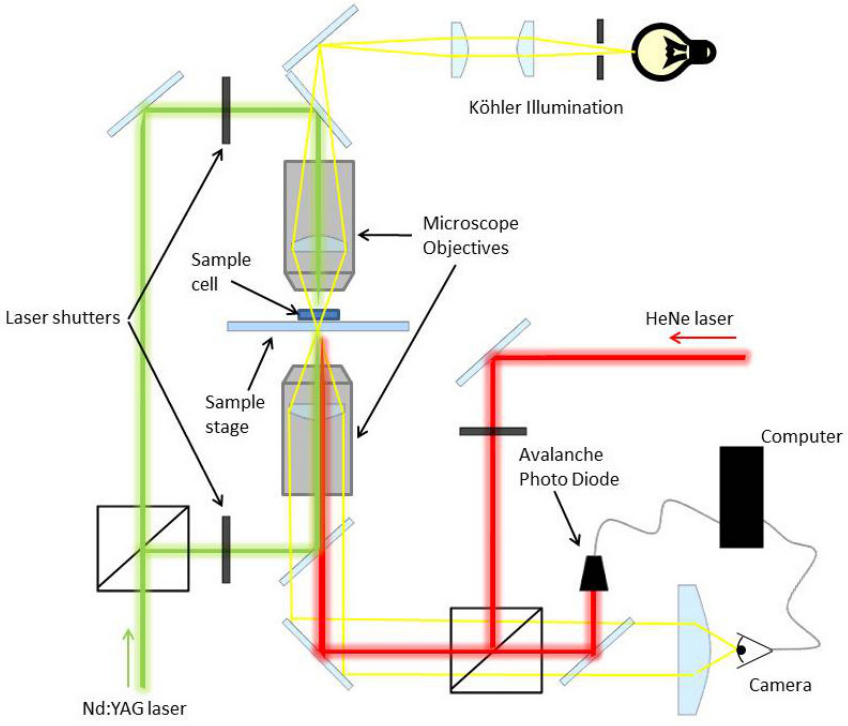

Figure 3.2.: This graphic shows a schematic overview over the main parts needed for the trapping of microspheres and measuring their sedimentation inside the sample cell. Note that, contrary to this depiction, the up-part of the trapping laser and the RICM laser are exactly coaxial when entering the microscope objective.

- The interference laser is named HNL020L and manufactured by THORLABS. This one is a HeNe laser with a wavelength of 633 nm and therefore is seen red. Its power ranges from two to four Milliwatt. After reflection it follows the beam path to a photo diode.

All three laser beams (HeNe laser as well as down- and up-part of the Nd:YAG laser) can be individually stopped by shutters.
The laser beams are focused by two microscope objectives made by Nikon. By careful adjusting the optical elements in the beam paths it is to achieve that both foci are at the exact same place in the sample cell. The two objectives differ in purpose and type:

- The upper objective is for focusing the down beam of the trapping laser. Since I only needed the up beam for my experiments, this objective was only needed for adjusting the system and focusing the microscope illumination. The type name reads Nikon T Plan SLWD 50x/0.40.
- The lower objective is used for focusing the up beam of the trapping laser and the interference laser as well as projecting the picture of the sample to the camera. The type name reads Nikon TU Plan ELWD 50x/0.60 B.

To measure the intensity of the interference an Avalanche Photo Diode (ADP130x, made by THORLABS) was used. Its signal was read by a computer where it was gathered and saved with a program written by Dominik Pilat in LabVIEW [11].
A digital camera (Marlin F-080B) recorded the proceedings in the focus of the objectives and sent its data to the computer where it was possible to observe the handling of the microspheres in realtime. That is important for successful trapping and measuring of beads. To get an image with good resolution a Köhler illumination was installed. The light source is a High Intensity Fiber Light Source OSL1-EC from THORLABS.
In the experiments it is needed to be able to move the focus in the sample cell in all three dimensions. Since the optical system is fixed once it is adjusted, we move the sample itself. This is done with a motorized stage 8MT167-25-MEn1 produced by Vision Lasertechnik für Forschung und Industrie GmbH.

3.2. The Performed Experiments and General Evaluation

I produced several samples by filling the sample cell with a medium in which the microspheres were dispersed. This cell was then put on the sample stage of the optical trap and I started measuring inside it. Per sample I conducted a series of sedimentations with four beads.
When I chose a microsphere via microscope, I first looked for irregularities and damage as far as it was possible. When the particle was found well suited it was pushed with the green trapping laser to the upper wall and followed with the focus by driving the motorized stage downwards.
When the bead did not rise further, because it is very close to the wall and the forces on it are in equilibrium, I switched off the trapping laser to allow the bead to sink down, measured the sedimentation velocity with RICM and after a certain time switched the laser on again to trap the same sphere for further probing. After I have done this five times I moved the focus to $d = 50\ \mu m$ and, with the same bead, repeated the procedure again five times, but this time I was able to measure the movement a little bit further away from the wall.
That I did for five different focus positions: at the upper wall of the sample cell, $D = 50\ \mu m$, $D = 100\ \mu m$, $D = 200\ \mu m$ and $D = 500\ \mu m$. D is the distance of the focus to the upper wall.
A recorded sedimentation is an interference pattern and therefore a plot of intensity versus time, see figure 3.3 for an example of a sedimentation at the wall. A sedimentation in the bulk is shown in figure 3.4. One can see that it is not just a straight signal but it shows a curvy envelope. Since the intensity of the backscattered laser beam is strongest when the bead is near the focus, this envelope occurs. The fact that there are further maxima may be caused by refraction effects of the ball lens, i.e. the microsphere in the beam.

To get the speed of a falling sphere I had to determine the time between two extrema in those interference pattern and plot the time coordinate against the travelled distance. The distance between two maxima can be calculated, see chapter 2.4 and is for water $d_{maxima} = 118,6797\ nm$. This plot is then fitted either with a linear fit, when the sedimentation was not recorded directly at the wall; or the integrated formula of Butt and Kappl, equation 2.8, when the sedimentation of the sphere started at the wall. See figure 3.5 for an example at the wall, 3.6 for an example in the bulk.
The slope of the linear fit gives the sedimentation velocity, while the fit parameter of the integrated Brenner formula is $\alpha = \frac{6\pi\eta}{F}$.

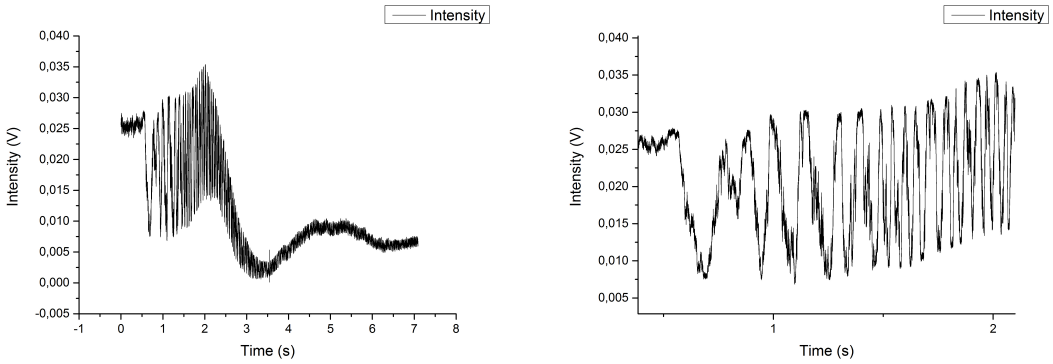

Figure 3.3.: On the left side is an example for a sedimentation with focus at the wall of the third sample, first bead. Plotted is the intensity of the interference signal versus time. One can easily see that at the start of the sedimentation the particle falls slower (i.e. the intensity maxima are wider apart), because of the higher drag at the wall.
On the right side is a close up of the first few maxima shown.

3.3. Checking for Possible Thermal Effects

As mentioned before in chapter 2.1.1, the viscosity of a liquid is highly dependent on the temperature of this liquid. While the room temperature was constantly controlled with a thermometer and averaged $T_{room} = 21,2 \pm 0,4$ °C, it is hardly possible to tell which temperature the trapped bead and the surrounding medium have.
It is conceivable that by absorption of photons of the laser the microsphere gets hotter and therefore heats the surrounding medium. In this case would the viscosity, experienced by the sphere, be lower than expected and thus the bead would sediment faster.
I tested this behaviour with a solution of $0,1\ \frac{mmol}{l}$ NaCl in water, in which beads made by Bangs Laboratories, Inc. (radius $r = 2,53\ \mu m$) were dispersed.
In the graphs of figure 3.7 on 14 are the speed values at different laser attenuations for two different beads shown. The corresponding data can be found in table A.1. If heating played a role, than the measurements conducted with a lower attenuation should yield a higher velocity. But as one can see in the figures, the values scatter arbitrarily around a mean and do not follow this trend. Therefore I suppose that no noticeable heating of the beads takes place. That means for all following experiments that it is not crucial to perform with the same laser intensity.

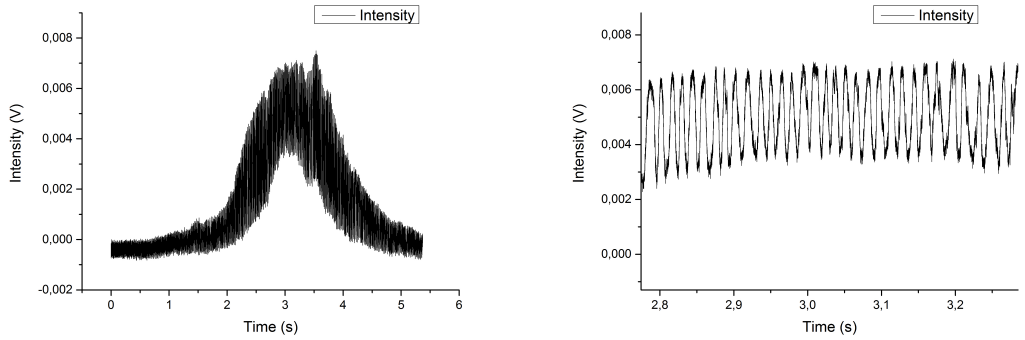

Figure 3.4.: On the left side is an example for a sedimentation with focus at $D = 200\mu m$ of the second sample, fourth bead. The big peak indicates the position of the focus.
On the right side is a close up of the maxima in the focus shown.

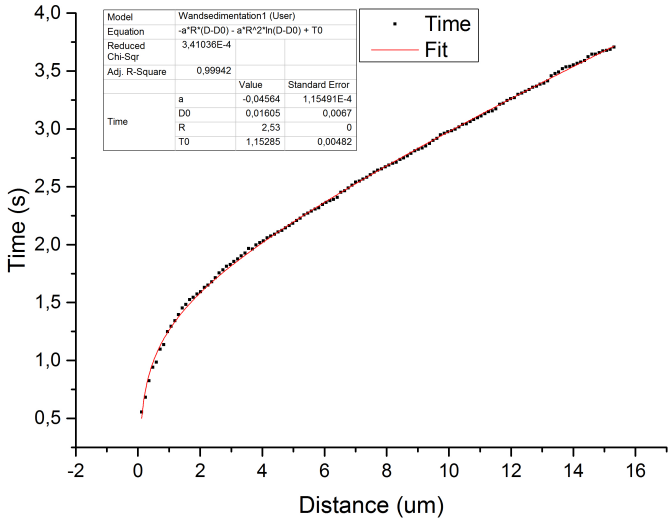

Figure 3.5.: The plotted sedimentation of figure 3.3, time versus distance. The plot was fitted with the integrated formula, equation 2.8.

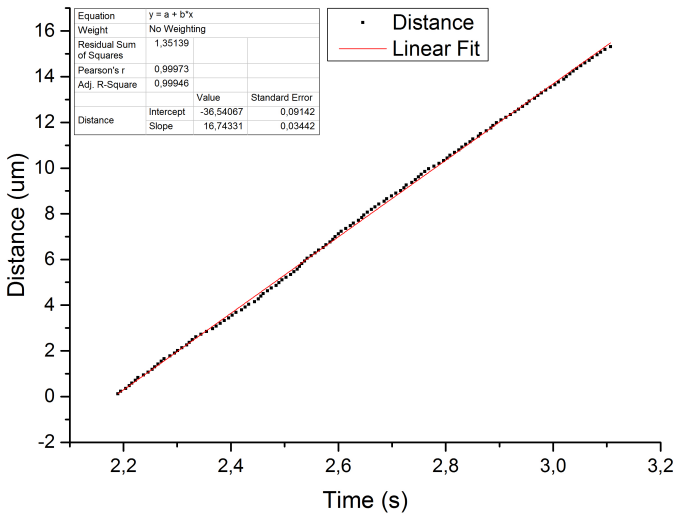

Figure 3.6.: The plotted sedimentation of figure 3.4, time versus distance. The slope of the linear fit is the sedimentation velocity.

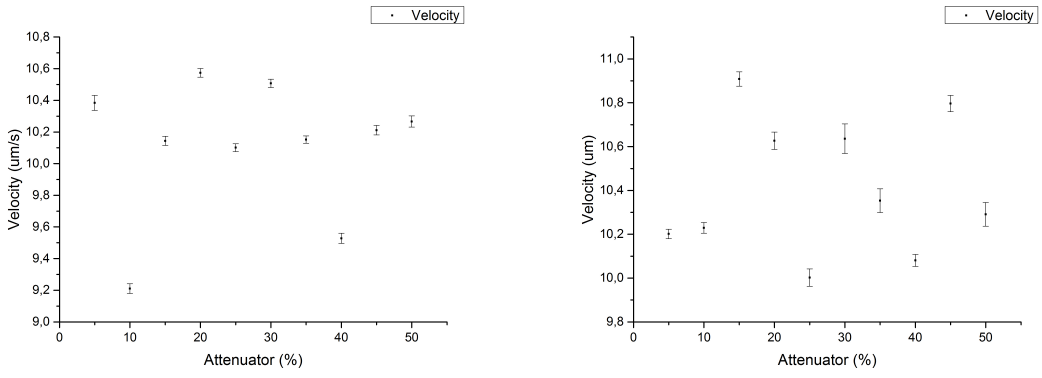

Figure 3.7.: Graphs of the data from table A.1. Sedimentation velocities against the trapping laser attenuation.

4. Evaluation

In this chapter I will discuss the collected data and its evaluation along with all experiments of my work.

4.1. Sedimentation in Water at the Wall and in the Bulk

The first task of my work was to compare sedimentations in water at the wall with sedimentations in the bulk. The first sample I produced for this task consisted of Duke Standard 9008 microspheres dispersed in a solution of $0,1\ \frac{mmol}{l}$ NaCl in pure water (impedance $18,2\ M\Omega cm$). The addition of salt is necessary to minimize adhesion caused by wall effects. Without it, the beads would stick to the wall once brought into contact with it.
The specifications of these micropsheres can be found on the corresponding data sheet and read as following:

Lot No.:	44222,
Mean radius:	$\bar{r}_{spec} = 4,00\ \mu m$ with
Standard deviation:	$\sigma = 0,45\ \mu m$,
Density:	$\rho_{spec} = 2,55\ \frac{g}{cm^3}$.

The manufacturers of those beads measure the density values and the radius distribution for every lot and send a Certificate of Calibration and Traceability with each order.

4.1.1. Duke Standard 9008 Microspheres

In my preparations and first trials I soon found out that the biggest statistical error is given by the size of the chosen beads. That is because of the broad distribution of diameter given by the manufacturer and the fact that it is hardly possible to differentiate by eye between different sizes of beads via the microscope. In the end you never know which exact diameter to assume when performing the calculations. There are three optional approaches to get a radius for the used beads.
The first approach is to simply calculate with the radii given by the manufacturer of the microspheres. But then you have a big error to consider since the standard deviation of the radius of the Duke Standard 9008 is stated with $\sigma = 0,45\ \mu m$. And since the measurements with the optical trap are single particle experiments, they can not deliver reliable statistics and this method would yield outcomes with a vast uncertainty.
The second approach is to take photos of the beads through the microscope and later determine the diameter of them with the program ImageJ (Image Processing and Analysis in Java, see [9]). The problem with this procedure is that the microspheres act as ball lenses and therefore refract the light of the microscope illumination in a certain way, so that in the pictures taken the edges of the beads are diffused. In combination with a not optimal optical resolution it is hard to tell where the glass ends and to measure an exact diameter. But an advantage to the

first method discussed you get an individual diameter for each bead, which should lead to a higher reliability of the outcomes.
The last possible solution to get reliable values for the microsphere radii is to assume that for sedimentations at a distance $D = 500\ \mu m$ no wall effects need to be considered, because the Brenner factor for this distance nearly shrinks to $\lambda_B = 1$ since a short calculation with equation 2.6 yields

$$\lambda_B = 1 + \frac{r_s}{d} = 1 + \frac{8\ \mu m}{500\ \mu m} = 1,016. \tag{4.1}$$

Therefore I was able to determine values for the radii of the beads out of the sedimentations at $D = 500\ \mu m$, which I measured for every singe bead, using a combination of 4.5 and 2.3, which yields

$$r_s = \sqrt{v_s \eta \frac{9}{2g(\rho_s - \rho_w)}}\ . \tag{4.2}$$

While the last method gives us the first trustworthy values for the individual radii, it is important to know that these values contain errors, which is highly dependent on the error of the assumed density of the microsphere. Is the density lower than assumed, than the so determined radius will be lower, too.
For all evaluations of the sedimentations in water I used the last method, the resulting radii are shown in table 4.1.

Table 4.1.: Sedimentation Speed at $d = 500\ \mu m$ in water and resulting radius for the Duke Standard 9009. Assuming a density of $\rho = 2,55\ \frac{g}{cm^3}$ and a viscosity of $\eta_{lit} = 1,00\ mPa \cdot s$. The last column shows the mean radius with its standard deviation.

Bead No. 1	$v_s\ [\frac{\mu m}{s}]$	37,41	36,47	38,05	37,21	36,53	Mean:
	$r\ [\mu m]$	3,33	3,29	3,36	3,32	3,29	3,32 ± 0,03
Bead No. 2	$v_s\ [\frac{\mu m}{s}]$	36,22	35,98	34,70	33,52	33,71	Mean:
	$r\ [\mu m]$	3,27	3,26	3,20	3,15	3,16	3,20 ± 0,05
Bead No. 3	$v_s\ [\frac{\mu m}{s}]$	53,63	56,89	55,87	56,37	57,39	Mean:
	$r\ [\mu m]$	3,98	4,10	4,07	4,08	4,12	4,08 ± 0,05
Bead No. 4	$v_s\ [\frac{\mu m}{s}]$	49,15	47,96	47,31	47,70	47,44	Mean:
	$r\ [\mu m]$	3,81	3,77	3,74	3,76	3,75	3,76 ± 0,03

With those calculated radii I was able to determine values for the viscosity for each sedimentation at the distances $D = 50\mu m$, $D = 100\mu m$ and $D = 200\mu m$. For the first sample this is shown in graph 4.1 and the corresponding table A.2. Actually it is not the viscosity η that was determined, but an effective viscosity containing the simplified Brenner factor $\eta^* = \eta \cdot \lambda_B$. The viscosity η itself should not change without changing the liquid or alternating the temperature, but only the approximated Brenner factor will change due to longer distances to the wall. I will for better reading purposes use the term viscosity for both and make with help of η and η^* clear which one is meant.
In table A.2 one can see, next to the sedimentation velocities and the resulting viscosities η^* the corresponding mean viscosity $\bar{\eta}^*$ of the particular bead and distance to the upper wall. The standard deviation of these mean viscosities ranges roughly between 1 % and 3 %. That

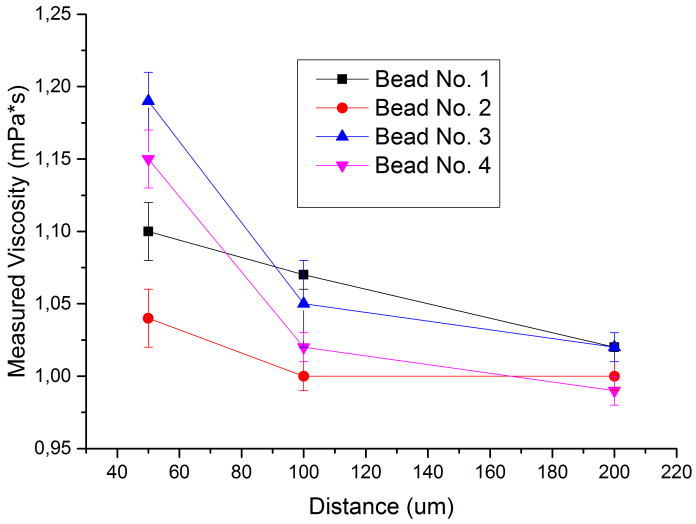

Figure 4.1.: Depiction of the measured viscosities at different focus positions, for all four beads of the Duke Standard 9008 sample in water. The complete data of these measurements is shown in table A.2. The connections between the data points are lines to guide the eye and have no mathematical reason.

means that the values of the different measurements scatter narrowly around the mean, what speaks for a high reproducibility of the outcomes and shows the high stability of the system itself.
As expected, the viscosities η^* nearer the wall are bigger than far away in the bulk. To examine whether the values correspond quantitatively with the simplified Brenner factor I will make a few simplifications. The first one is to calculate the mean viscosity for a certain distance over all beads. This leads

for $D = 50\ \mu m$ to $\bar{\eta} = (1,12 \pm 0,06)\ mPa \cdot s$,
for $D = 100\ \mu m$ to $\bar{\eta} = (1,03 \pm 0,03)\ mPa \cdot s$ and
for $D = 200\ \mu m$ to $\bar{\eta} = (1,01 \pm 0,02)\ mPa \cdot s$.

Then, for the calculation of the Brenner factor I will use the mean radius of the four Beads $\bar{r} = 3,59 \pm 0,35$. Since the viscosity η of water can be assumed with $\eta_{water} = 1,00\ mPa \cdot s$ the product is simplified to

$$\eta^*_{lit} = \lambda_B \cdot \eta_{water} = (1 + \frac{r}{D}) \cdot 1,00\ mPa \cdot s = (1 + \frac{r}{D})\ mPa \cdot s\ . \tag{4.3}$$

It has to be understood that these distances describe the position of the focus but not necessarily the exact distance of the measurement to the upper wall since it is not always possible to obtain the correct position of the focus out of the interference patterns. Furthermore the bead itself is travelling more than fifteen micrometers downwards over the measurement. Thus I assume an error of $\Delta D = 10\ \mu m$. The equation 4.3 has a noticeable error, which can be calculated with

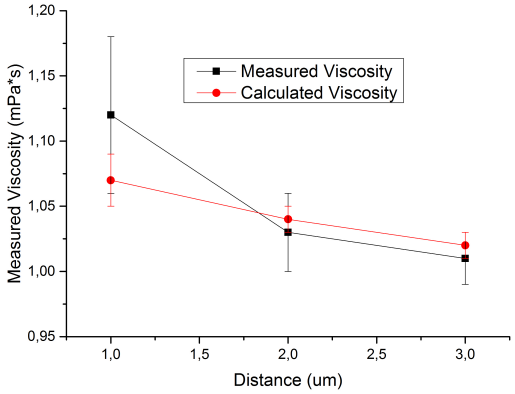

Figure 4.2.: Plot of the measured viscosity η^* of the first sample.. The connections between the data points are lines to guide the eye and have no mathematical reason.

$$\Delta\eta^*_{lit} = \eta_{water}\sqrt{\left(\frac{1}{D}\Delta r\right)^2 + \left(\frac{r}{D^2}\Delta D\right)^2}\ . \tag{4.4}$$

It yields

for $D = 50\ \mu m$ to $\eta^*_{lit} = (1,07 \pm 0,02)\ mPa \cdot s$,
for $D = 100\ \mu m$ to $\eta^*_{lit} = (1,04 \pm 0,01)\ mPa \cdot s$ and
for $D = 200\ \mu m$ to $\eta^*_{lit} = (1,02 \pm 0,01)\ mPa \cdot s$.

For a better overview in the following discussion, these values are shown in graph 4.2.
First, one can say that the measured values are not that far off. The measured viscosities η^* for the two greater distances are less than one percent too small. But the value nearer the wall is roughly five percent too big. The main reason for this difference may be that I evaluated the interference peaks which came chronologically after the peaks in the focus. As mentioned above it is a major error to not evaluate in the focus. But then again the standard deviation of the first distance of five percent is quite big and therefore the criterion lies within the error margin.
The chronological first part of the experiments, namely the sedimentation directly beginning at the upper wall, will be discussed now because there a different approach is required. As mentioned above, the wall sedimentations were fitted with the integrated simplified Brenner formula, see chapter 2.1.3. Therefore I did not get a sedimentation velocity as a fitting parameter, but the coefficient $\alpha = \frac{6\pi\eta}{F_D}$. F_D is the drag force and is to be equalled with the difference of buoyancy and the gravitational force:

$$F_D = F_{grav} - F_{buoy}\ . \tag{4.5}$$

Reorganizing yields the following expression for the viscosity η:

$$\eta_{water} = \frac{gV(\rho_B - \rho_{water}\alpha)}{6\pi}\ , \tag{4.6}$$

with V: the volume of the bead.
It is to consider that in this equation the resulting viscosity should be the viscosity η of water because the Brenner factor is only included in the drag force F_D, which got replaced with equation 4.5. The calculated values are shown in table 4.2.

Table 4.2.: Fitting parameter α at the wall and the resulting values for the viscosity η of the Duke Standard 9000 in water.

Bead No. 1	$\alpha\ [10^{-6}\frac{s}{m^2}]$	-9,02	-9,17	-8,97	-9,201	-9,24	Mean:
	$\eta\ [mPa \cdot s]$	1,11	1,13	1,10	1,13	1,14	1,12 ± 0,01
Bead No. 2	$\alpha\ [10^{-6}\frac{s}{m^2}]$	-9,21	-9,63	-9,65	-9,65	-9,27	Mean:
	$\eta\ [mPa \cdot s]$	1,03	1,08	1,08	1,08	1,04	1,06 ± 0,02
Bead No. 3	$\alpha\ [10^{-6}\frac{s}{m^2}]$	-4,57	-4,61	-4,58	-4,61	-4,56	Mean:
	$\eta\ [mPa \cdot s]$	1,04	1,05	1,04	1,05	1,04	1,05 ± 0,01
Bead No. 4	$\alpha\ [10^{-6}\frac{s}{m^2}]$	-5,69	-5,48	-5,71	-5,70	-5,75	Mean:
	$\eta\ [mPa \cdot s]$	1,03	0,99	1,03	1,03	1,04	1,02 ± 0,02

One can see that these outcomes do not meet the expectations. All the calculated values for the viscosity η are too high and spread widely around their arithmetic centre, which is $\bar{\eta} = (1,06 \pm 0,04)\ mPa \cdot s$. Thus, this mean value is six percent higher than the expected value, but considering the error margins not that far off.
While for a single bead the results lie very closely around their mean and therefore are reproducible, comparison between all four beads show that with a new bead the situation changes and the result is different to those before. This may be caused by irregularities on the surface of the used microsphere. Little spikes or areas with another radius of curvature will lead to a situation, where the equation 2.7 yields incorrect outcomes. One has to consider that, when the pushing force of the laser and the rejection from the wall are in equilibrium, the bead is only a few hundred nanometers away from the surface and thus even little surface irregularities have a major influence on the outcome of the experiment. Not only irregularities on the microsphere are to be considered, but those on the wall of the sample cell can influence the way in which water flows in or out the gap between the sphere and the wall.
Another possible reason for the six percent difference is the change made by Butt and Kappl to the original Brenner formula by approximating the Brenner factor as seen in equation 2.6. This approximation may lead to greater uncertainties the nearer to the wall the viscosity is measured.
As these measurements yielded good results, which means they were close to the expected expected values, for measurements at the wall, in the bulk as well as in between, I wanted to test the optical trap with a different set of beads.

4.1.2. Microspheres of Bangs Laboratories, Inc.

I produced two sample solutions of $0,1\ \frac{mmol}{l}$ NaCl in pure water (impedance $18,2\ M\Omega cm$) in which I dispersed microspheres of the company Bangs Laboratories, Inc..
The first sample contains microspheres with the following specifications, taken from their product sheet:

Type No.:	SS06N,
Lot No.:	10936,

Mean radius:	$\bar{r}_{spec} = 2,53\ \mu m$ with
Standard deviation:	$\sigma = 0,22\ \mu m$,
Density:	$\rho_{spec} = 2,00\ \frac{g}{cm^3}$.

The microspheres of the second sample have following specifications:

Type No.:	SS06N,
Lot No.:	10096,
Mean radius:	$\bar{r}_{spec} = 3,23\ \mu m$ with
Standard deviation:	$\sigma = 0,31\ \mu m$,
Density:	$\rho_{spec} = 2,00\ \frac{g}{cm^3}$.

Contrary to the producer of the Duke Standard 9008 microspheres Bangs Laboratories, Inc. give just an estimated value for the density of the beads.
This part of the evaluation will handle both experiments in parallel.
Overall, I used the same procedure for my evaluation as for the Duke Standard 9008 sample. From the last sedimentation at $D = 500\ \mu m$ the radius of each bead was determined, which is to be seen in tables A.3 and A.4 in the appendix. For the first sample the mean radius is $\bar{r} = (2,12 \pm 0,05)\ \mu m$, where it should be around $r_{spec} = 2,53\ \mu m$ and thus is 16 % too small. The same applies for the second sample, where the mean radius is $\bar{r} = (2,12 \pm 0,05)\ \mu m$ and the given radius is $r_{spec} = 2,53\ \mu m$. The difference comes again to 16 %.
I think the reason for that lies mainly in the by the manufacturer given value for the density $\rho_{spec} = 2,0\ \frac{g}{cm^3}$, which was used to calculate the forces on the beads. Again, the calculated radii are equivalent radii of microspeheres with this density. It seems that the beads have a much lower density than stated. Using the equation

$$\bar{\rho}_{bead} = \frac{9\bar{v}\eta}{2gr^2} + \rho_{medium} \tag{4.7}$$

I can calculate which density would come out when I assume the by the manufacturer given radius. For the microspheres with radius $\bar{r}_{spec} = 2,53\ \mu m$ it yields $\bar{\rho}_{2,53} = 1,74\ \frac{g}{cm^3}$ and for $\bar{r}_{spec} = 3,23\ \mu m$ it yields $\bar{\rho}_{2,53} = 1,70\ \frac{g}{cm^3}$. Both values are noticeably smaller than the stated density, but interestingly are close to each other.
The next step was again to determine the viscosities η^* from the three other bulk sedimentations, which is graphically shown in figures 4.3 and 4.4. The first thing one can see is that the outcomes of the single sedimentations scatter less narrowly around their mean than with the Duke Standard 9009 microspheres: for the third sample with radius $r_{spec} = 3,23\ \mu m$ the standard deviation goes up to four percent, while for the second sample with radius $r_{spec} = 2,53\ \mu m$ it goes up to six percent.
The reason for this increased instability with decreased radius of the bead lies in the fact that the sinking velocity is proportional to the squared radius $v_s \sim r^2$. A higher velocity leads to a lower vulnerability of the trajectory to fluctuations caused by Brownian motion and therefore the interference signal is much cleaner.
Not a single bead of the second sample shows the expected decrease of the Brenner factor with increasing distance to the upper wall. The values are jumping around arbitrarily, as it seems. I think there a few possible reasons for this:

- As mentioned above leads a smaller radius to a higher vulnerability to Brownian motion and thus to unstable outcomes.

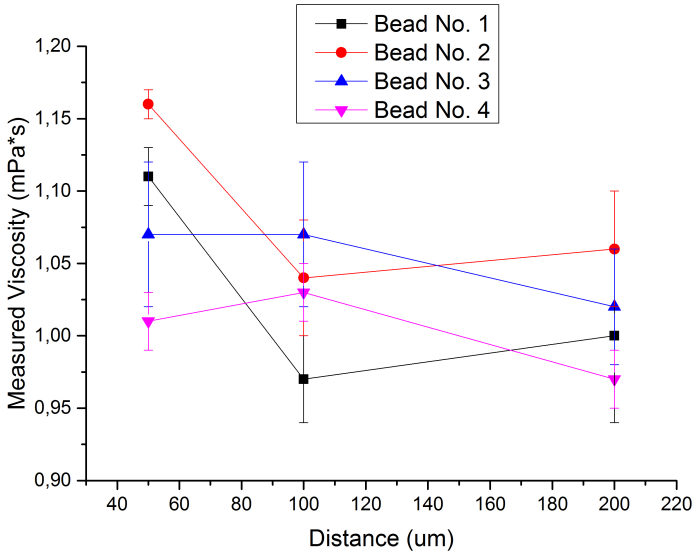

Figure 4.3.: Depiction of the measured viscosities at different focus positions, for all four beads of the Bangs Laboratories, Inc. sample with $r_{spec} = 2,53\ \mu m$ in water. The complete data of these measurements is shown in table A.5. The connections between the data points are lines to guide the eye and have no mathematical reason.

- It is possible that the interference laser's radiation pressure on the bead slows its sedimentation down. But that would happen with all samples, therefore we can ignore it when looking for sources of error for these particular Bangs Laboratories, Inc. samples.
- Short-term thermal effects could play a role. Heating from the Köhler illumination is a long term effect and thus leads to an equilibrium, but the trapping laser may cause local heating while it is switched on and thus small vortices and locally alternated viscosities can influence the measurements. For sure, this is not sample related and can be the case with Duke micorspheres as well, but since those are heavier they may be less influenced by it.
- Calculating the radii showed that the density of the beads may be much smaller than stated. That could be caused by porosity of the material. Smaller densities would yield slower velocities.

I wanted to examine the beads of the second sample with Bangs Laboratories, Inc. microsphere of radius $r = 2,53\ \mu m$ in more detail to better understand the nature of their composition and thus can estimate the gravity of the last error source.
Maren Müller of the MPIP took pictures with an SEM of six single beads that were glued to an AFM cantilever beforehand by Michael Kappl. While SEM allows to examine the beads with high resolutions and thus determining the radius, AFM can give me the mass of a single bead.
After Michael Kappl glued the beads on the cantilever in the AFM he also indirectly measured their mass by using the resonance frequency of the cantilevers, like it is described in [7]. The

Table 4.3.: Each bead with its corresponding mass, determined with AFM resonance frequency probing, radius, optically determined with an SEM, and calculated density.

Bead No. 1	$m_{bead}\ [kg]$	$r_{bead}\ [\mu m]$	$\rho_{bead}\ [\frac{g}{cm^3}]$
1	$(7,84 \pm 0,21)10^{-}14$	$2,39 \pm 0,1$	$1,37 \pm 0,35$
2	$(8,49 \pm 0,23)10^{-}14$	$2,39 \pm 0,1$	$1,49 \pm 0,35$
3	$(8,17 \pm 0,20)10^{-}14$	$2,41 \pm 0,1$	$1,39 \pm 0,36$
4	$(9,06 \pm 0,28)10^{-}14$	$2,51 \pm 0,1$	$1,37 \pm 0,43$
5	$(9.47 \pm 0,22)10^{-}14$	$2,44 \pm 0,1$	$1,56 \pm 0,39$
6	$(6,37 \pm 0,16)10^{-}14$	$2,43 \pm 0,1$	$1,06 \pm 0,30$

mass is needed for the determination of the bead densities. The outcomes are along the radii from the SEM shown in table 4.3.
A picture of the first bead in close up and the whole cantilever can be seen in figure 4.5. The other recordings are to be found in the appendix (figures A.1, A.2, A.3, A.4 and A.5). One notices that bead number one and four show obvious misshapes.
Except for the first bead, there were always two close up pictures taken, using two different detectors, a TLD (through lens detector) and an ETD (Everhart-Thornley detector). The first one I used to get the radii of the beads with help of the program ImageJ, the results are shown in table 4.3. Although this is only a small random sample one can see that the mean radius $\bar{r} = (2,43 \pm 0,04)\ \mu m$ is only four percent smaller than the stated radius, contrary to the calculated radii.
The so calculated densities for each bead are much smaller than the stated $\rho_{spec} = 2,0\ \frac{g}{cm`3}$, the mean value with its standard deviation is $\bar{\rho} = (1,38 \pm 0,16)\ \frac{g}{cm`3}$. The single results have vast error margins because these resonance frequency measurements are quite inaccurate (the part that makes it inaccurate is the determination of the spring constant k). Therefore the outcome of these measurements can only be taken as an additional hint to the lower dense consistency of the Bangs Laboratories, Inc. samples.
The second picture of beads two to six allow a qualitative examination of the surface structure of each bead (figure 4.6) for the second bead (the others can be found in the appendix figures A.6 and A.7). Overall, one can say that the surfaces are far from perfectly flat, but show a lot of small craters and look porous.
Those findings confirm my assumption that the density of the beads is far lower as stated due to porosity and therefore the sedimentation velocity of these beads is slower than it would be if the had the stated density.

In the case of the sample with radius $r_{spec} = 3,23\ \mu m$ one can see that the viscosities increase with greater distance and so follow at least qualitatively the expectations. In order to check for the quantitative correlation I repeated the procedure from before and calculated the mean values for the distances $\bar{\eta}^*$ and the expected value η^*_{lit} using the Brenner factor. This is shown in table 4.4 and in graph 4.7.
The outcomes of this experiment fit the expectations as good as the Duke microspheres, and in the case of the measurements at $D = 50\ \mu m$ even better. That can be explained by a better choice when guessing where the focus in the interference pattern lies, so that I actually evaluated the peaks at $D = (50 \pm 10)\ \mu m$. With roughly three to four percent

Table 4.4.: Comparison of mean values of viscosities for the third sample to expectations of the Brenner factor.

D in μm	50	100	200
$\bar{\eta}^*$ $[mPa \cdot s]$	$1,14 \pm 0,04$	$1,05 \pm 0,03$	$1,01 \pm 0,03$
η^*_{lit} $[mPa \cdot s]$	$1,13 \pm 0,02$	$1,06 \pm 0,01$	$1,03 \pm 0,01$
Deviation in %	1	1	2

standard deviation lie the results as closely around the means as with the Duke Standard 9009 microspheres.
The results of the wall sedimentations for the first and second sample are shown in tables A.7 and A.8 in the appendix. Again, the standard deviations are smaller with smaller radii. Here, too, the expected value for the viscosity is $\eta_{water} = 1,00 mPa \cdot s$. As one can see the measured values are up to 23 % higher. The mean viscosities are $\bar{\eta}_2 = 1,17 \pm 0,04$ and $\bar{\eta}_3 = 1,11 \pm 0,34$. That means they are 17 %, respectively 11 % to high.
While the third sample still gave appropriate results at the positions in the bulk, both Bang Laboratories, Inc. samples yielded worse outcomes compared to the Duke Standard 9008 sample for the wall sedimentation. Due to the fact that the Duke microspheres acted overall more as expected I used them for further experiments.

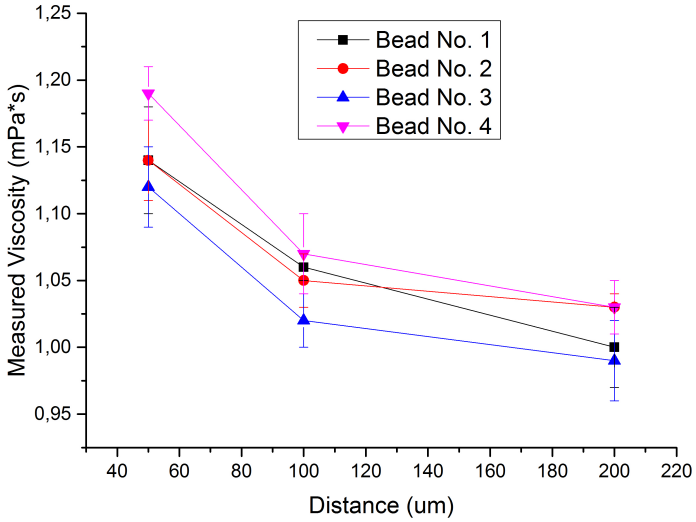

Figure 4.4.: Depiction of the measured viscosities at different focus positions, for all four beads of the Bangs Laboratories, Inc. sample with $r_{spec} = 3,23\ \mu m$ in water. The complete data of these measurements is shown in table A.6. The connections between the data points are lines to guide the eye and have no mathematical reason.

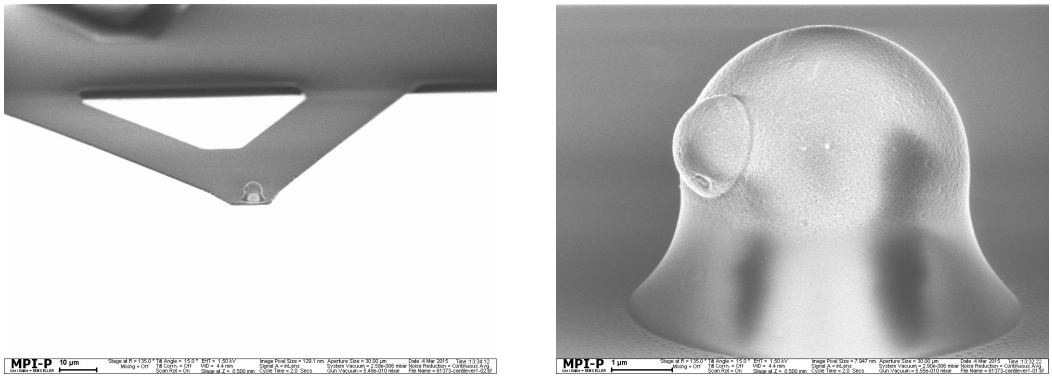

Figure 4.5.: Pictures taken with an SEM of the first Bangs Laboratories, Inc. bead. Left picture shows the whole cantilever and right one a close up of the bead.
Taken by Maren Müller.

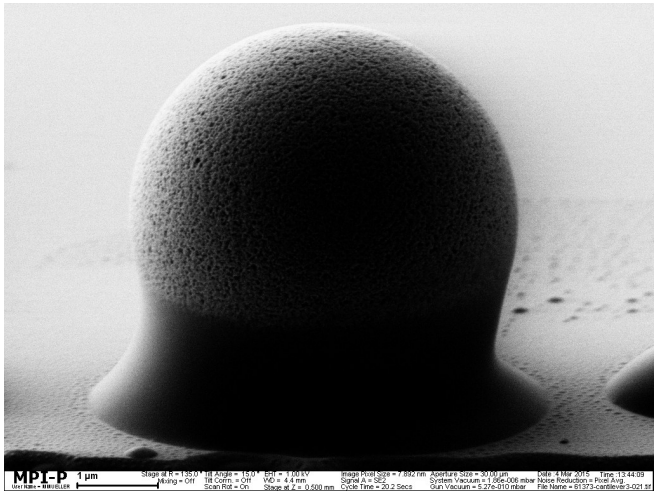

Figure 4.6.: SEM picture of the third bead, recorded with an ETD for better surveying the surface structure of the microspheres.
Taken by Maren Müller

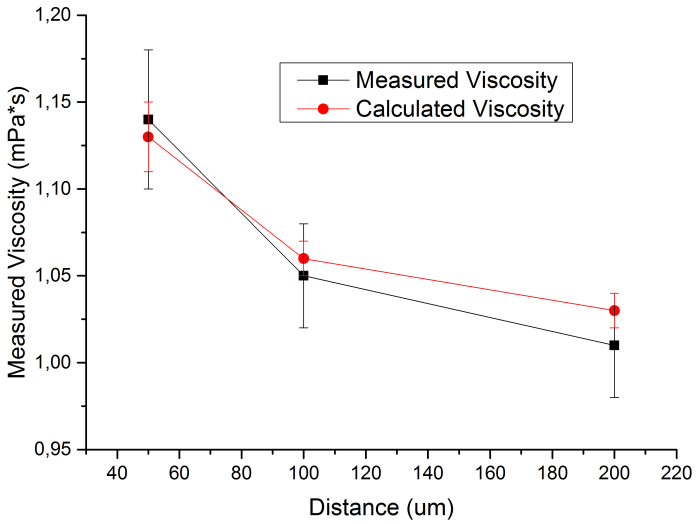

Figure 4.7.: Plot of the measured viscosity of the third sample. The connections between the data points are lines to guide the eye and have no mathematical reason.

4.2. Sedimentations in Aqueous Glycerol Solutions

For my experiments with higher viscosities I chose The Duke Standard 9008 microspheres, thus the specifications remain the same as for the first sample. I dispersed them in a solution of $0,1\ \frac{mmol}{l}$ NaCl in water where I added 20 %vol. glycerol to one sample and 40 %vol. glycerol to the other sample.
I measured both glycerol solutions with a ZEISS refractometer and found out that their refractive indices were low enough to allow optical trapping: water with 20 %vol. glycerol gave $n_{20\%} = 1,36$ and 40 %vol. glycerol gave $n_{40\%} = 1,39$, which seems to be reliable since pure glycerol has a refractive index of $n_{gly} = 1,4745$ [2]. I needed these values to calculate the travelled distance that is equivalent to running through the extrema of RICM (see 2.4). For sure these determined numbers contain an unknown systematic and a negligibly small statistical error. Because I measured all solutions with the same refractometer I can still compare my outcomes among themselves. Nevertheless, for absolute determination of viscosity I have to consider this systematic offset.
Additionally it is important to know the density of my solutions for the calculation of buoyancy. Therefore I weighed a small amount of the solutions $V = 1000\ \mu l$, measured with a blue Eppendorf pipette, which can contain 1000 μl and has a stated error of $\Delta V = 8\ \mu l$. The balance was named METTLER AE240 Zweibereichswaage and has a stated error of $\Delta m = 0,05\ mg$. That procedure yielded the following densities

20 %*vol.* glycerol: $\rho_{20\%} = (1,067 \pm 0,009)\ \frac{g}{cm^3}$
40 %*vol.* glycerol: $\rho_{40\%} = (1,132 \pm 0,009)\ \frac{g}{cm^3}$.

Again, these values seem reliable because the density of pure glycerol is $\rho_{gly} = 1,26\ \frac{g}{cm^3}$ [5].

In this task I faced the problem that the velocity η for the mixtures is unknown and so I was not able to determine the radius of a particular bead by evaluating the sedimentation at $D = 500\ \mu m$, thus I had to use the images taken with the microscope and again the program ImageJ.
What I have done first was to look at the beads of the first sample with Duke Standard 9008 microspheres in water, where I determined the radii from the last bulk sedimentation, and looked at their recordings in ImageJ, to learn how to put the measuring ring in the microspheres. This is shown in figure 4.8. Next, for the beads of sample four and five I applied the measuring function of ImageJ in the same way. The corresponding images can be found in the appendix (figures A.8 and A.9) and the results in table 4.5. Note that this determination succumbs a noticeable error due to blurriness and refraction effects. I estimated the error of the diameter measurement to $\Delta d = 0,4\ \mu m$ and thus the radius error is $\Delta r = 0,2\ \mu m$, which is about five percent of the total value.
As one can see, the mean radius of both samples lies very close to the stated radius of the manufacturer. However, the standard deviation is quite big and that shows that the single

Table 4.5.: Optically determined radii of each bead of both glycerol containing samples in units of µm.

	Bead No. 1	Bead No. 2	Bead No. 3	Bead No. 4	Mean:
4^{th} sample	$4,34 \pm 0,4$	$3,32 \pm 0,4$	$4,11 \pm 0,4$	$4,11 \pm 0,4$	$\bar{r} = (3,97 \pm 0,39)\ \mu m$
5^{th} sample	$3,61 \pm 0,4$	$4,15 \pm 0,4$	$4,07 \pm 0,4$	$4,94 \pm 0,4$	$\bar{r} = (3,94 \pm 0,21)\ \mu m$

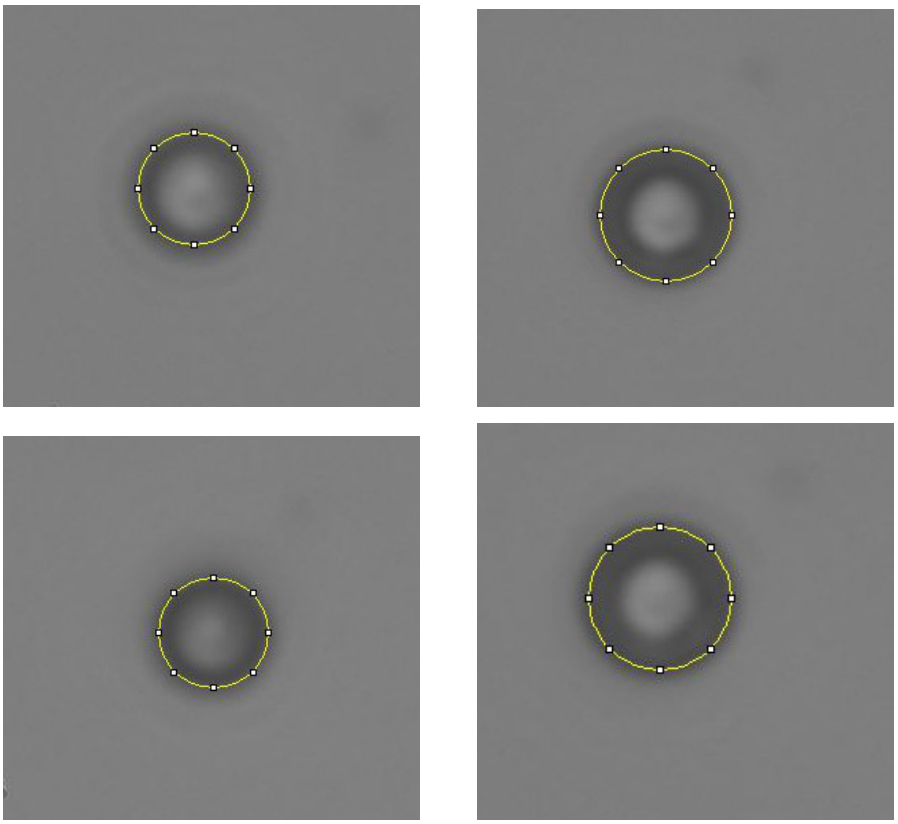

Figure 4.8.: Beads of first sample, processing and diameter measuring (yellow circle) with ImageJ.

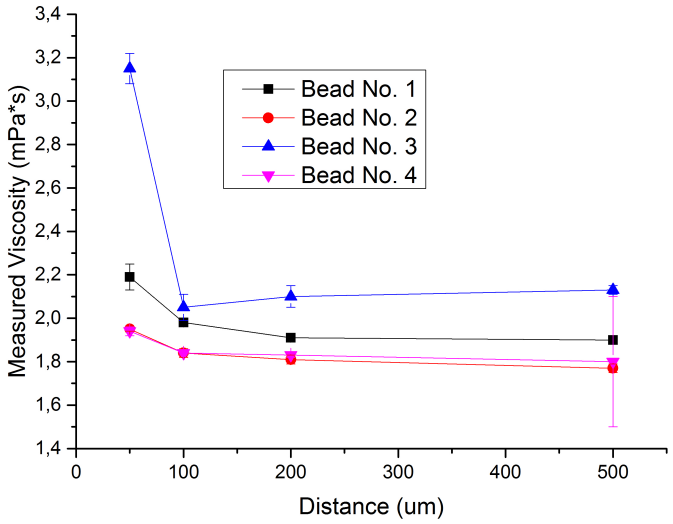

Figure 4.9.: Depiction of the measured viscosities at different focus positions, for all four beads of the Duke Standard 9008 sample in 20 %vol. glycerol. The complete data of these measurements is shown in table A.9. The connections between the data points are lines to guide the eye and have no mathematical reason.

values spread widely around their centre. With these radii I was able to analyse the collected data and calculate the viscosities. For the distances $D = 50\mu m$, $D = 100\mu m$, $D = 200\mu m$ and $D = 500\mu m$ the results for the 20 % glycerol solution are shown in figure 4.9, and for the 40 % glycerol solution in figure 4.11.
First I will discuss the sample with 20 %vol. glycerol. Using the formula of Cheng, a specific viscosity of $\eta_{20\%,lit} = 1,99\ mPa\cdot$ is expected, which should be met with the bulk sedimentation at $D = 500\ \mu m$.
A first look at the values in table A.9 reveals that they behave in the anticipated way: the viscosity values η^* get lower the farer from the wall they were measured and the last value of each bead lies in proximity to $\eta_{20\%,lit}$. The standard deviations of the mean values are bigger than for sample three, but that is easily understandable as the microspheres sediment slower, due to the higher viscosity η of the mixture, and therefore the trajectory suffers from Brownian motion. A quantitative comparison of the mean values for each distance to the Brenner factor calculated with the mean radius is shown in table 4.6, a graph in figure 4.10.
The first thing that one can see is that the standard deviation of each distance is very big, ranging from 5 % to 21 %. That is caused by the very different values for the viscosities η^* calculated from each microsphere. I suppose the reason for that variation is the determination of the radius out of the microscope images, which is very precarious.
Except for $D = 50\ \mu m$ are all measured viscosity values η^* to small, meaning the microspheres were to fast. The most obvious reason for that, assuming that the radius was correctly determined, is that the density stated by the manufacturer is too low, or the ratio of the glycerol solution was not exactly 20 %. Most likely is a combination of both. Another possible

Table 4.6.: Comparison of mean values of viscosities $\eta^*$for the Duke Standard 9008 sample in 20 %vol. glycerol to expectations for the Brenner factor.

$D\ [\mu m]$	50	100	200	500
$\bar{\eta}^*\ [mPa \cdot s]$	$2,31 \pm 0,5$	$1,93 \pm 0,1$	$1,92 \pm 0,12$	$1,90 \pm 0,14$
$\eta^*_{lit}\ [mPa \cdot s]$	2,14	2,07	2,03	2,01
Deviation in %	+8	-7	-5	-5

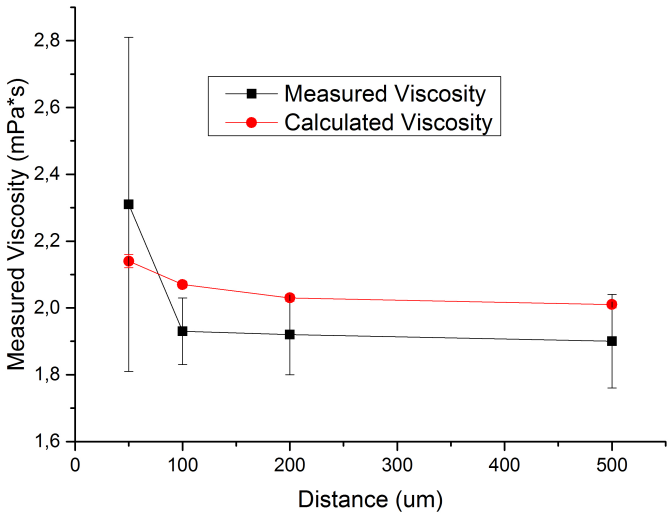

Figure 4.10.: Plot of the measured viscosity η^* of the fourth sample with 20 % glycerol. The connections between the data points are lines to guide the eye and have no mathematical reason.

reason could be the unknown systematic error made by the determination of the refraction index and thus a wrongly calculated sedimentation velocity.
The cause for the much to high value for $D = 50\ \mu m$ can be seen in table A.9: the outcomes for the third bead at this position spread around a centre value which is roughly 50 % higher than for the other beads. Then it drops to $\eta_{100m} = 2,05\ mPa \cdot s$ and, interestingly, rises again to $\eta_{500m} = 2,13\ mPa \cdot s$. The most likely reason for that is a misshaped bead, although it looks round and well shaped in figure A.8.

Table 4.7.: Fitting parameter α at the wall and the resulting values for the viscosity η of the fourth sample.

Bead No. 1	$\alpha\ [10^{-6}\frac{s}{m^2}]$	-7,21	-7,16	-7,44	-7,51	-7,45	Mean:
	$\eta\ [mPa \cdot s]$	1,89	1,88	1,95	1,91	1,96	1,93 ± 0,04
Bead No. 2	$\alpha\ [10^{-6}\frac{s}{m^2}]$	-13,99	-13,69	-15,70	-15,51	-15,60	Mean:
	$\eta\ [mPa \cdot s]$	1,65	1,61	1,85	1,82	1,83	1,75 ± 0,01
Bead No. 3	$\alpha\ [10^{-6}\frac{s}{m^2}]$	-8,91	-9,04	-10,65	-10,50	-10,74	Mean:
	$\eta\ [mPa \cdot s]$	1,99	2,02	2,38	2,34	2,40	2,22 ± 0,18
Bead No. 4	$\alpha\ [10^{-6}\frac{s}{m^2}]$	-8,15	-8,07	-8,47	-8,37	-8,32	Mean:
	$\eta\ [mPa \cdot s]$	1,82	1,80	1,89	1,87	1,86	1,85 ± 0,21

The viscosity values η determined by the wall sedimentations shown in table 4.7 scatter around the mean value $\bar{\eta} = (1,94 \pm 0,21)\ mPa \cdot s$, what is very close to the expected value. But in the context of the values for the bulk viscosities η^* , which where too low, it is clear that this outcome can not be trusted. It rather should be compared to the mean viscosity at $D = 500\ \mu m$, which is $\bar{\eta}^*_{500\mu m} = 1,90 \pm 0,14$, and there the discrepancy is about two percent, which is in accordance with earlier outcomes.
Nevertheless, the overall high standard deviations of this sample show the high insecurities in these experiments.
For the last examined sample with 40 % glycerol the expected viscosity is $\eta_{40\%,lit} = 4,83\ mPa \cdot s$. In figure 4.11 are the outcomes shown and in table A.11 one can see the comparison between mean viscosity values for each distance and the calculated ones, the corresponding graph in figure 4.12.
Again, the measured velocities of the microspheres were much higher then expected and thus the viscosities η^* about 20 % to low. This is similar to the outcomes of the fourth sample, however, this time the difference is bigger. Therefore I suppose that the main sources of the shift are the determination of the refraction index and the possibly inaccurate mixing ratio of glycerol and water, as the density of the beads should be the same as in sample four.
In table A.12 are the outcomes of the sedimentation at the wall listed together with the resulting viscosity values. Comparison of the mean $\bar{\eta}_{wall} = 3,83 \pm 0,1$ to the bulk sedimentation shows that it is roughly two percent too high, which is again in good accordance to the outcomes of the other experiments.
In all performed experiments the values for the viscosity η, that were determined with the sedimentations at the wall, were roughly about five percent too high. The constancy of this phenomenon suggest that it is not caused by the changes made to the system (i.e. different beads and solutions), but that at least the tendency of a too high value near the wall is generally valid.
One possible cause for this, as mentioned before, may lie in the simplification of the Brenner factor. It seems that its error gets bigger the closer to the wall the measurement was performed.

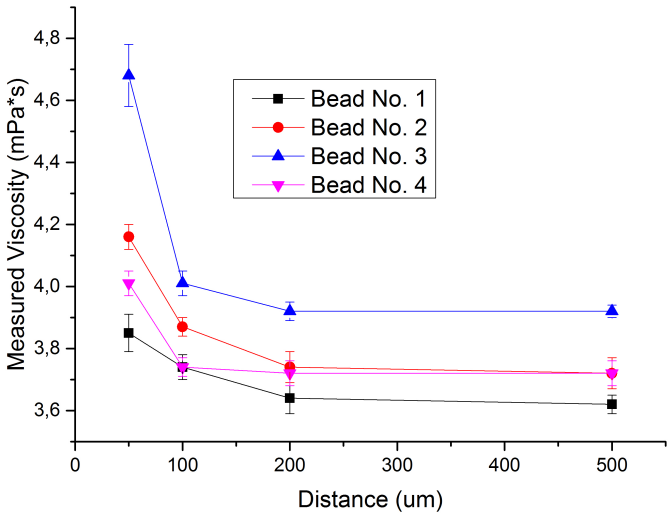

Figure 4.11.: Depiction of the measured viscosities at different focus positions, for all four beads of the Duke Standard 9008 sample in 40 %vol. glycerol. The complete data of these measurements is shown in table A.10. The connections between the data points are lines to guide the eye and have no mathematical reason.

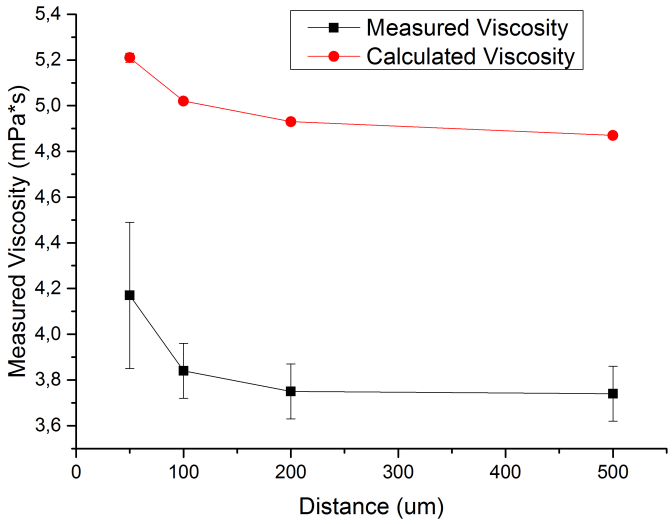

Figure 4.12.: Plot of the measured viscosity of the fifth sample with 40 % glycerol. The connections between the data points are lines to guide the eye and have no mathematical reason.

5. Conclusion and Outlook

After measuring the sedimentations of three different kinds of microspheres dispersed in three distinct solutions with the optical trap in combination with RICM I was able to evaluate the properties of measurements based on a comprehensive set of data. With the following words I will summarize my findings, make conclusions and give an insight of my thoughts about future research on this optical trap.
First, using the literature value for the viscosity of water to get the microsphere radius, I showed that it then is possible to get the viscosity of water with a deviation from the expected value of less than one percent ot of my measurements. That means the outcomes are consistent and not arbitrary. The survey of the sedimentations via RICM is precise enough to resolve the difference in viscosities of less then two percent between $D = 100\ \mu m$ and $D = 200\ \mu m$ for the first sample.
When raising the viscosity of the medium by adding glycerol to water we saw that the measured values admittedly were up to twenty percent lower than the expectations, but this discrepancy is most likely caused by a vague ratio of mixture in the glycerol solution. Further, the measurements get slightly more inaccurate due to a slower sedimentation velocity of the microspheres.
The fact that my measurements on all samples yielded outcomes that follow the expectations of the effect that the near wall has on the flow shows the high precision which one can reach while measuring with the combination of optical trapping and RICM. On the other hand it is possible to give accurate values for viscosities, as we have seen in the first measurements in water. However, in order to gain a high accuracy one has to know the radius of the microspheres along with their density.
While measuring with the microspheres of Bangs Laboratories, Inc. I realized that they behaved not as expected as their sedimentation velocity was to slow. My assumption that their density is at least ..... percent lower than stated by the manufacturer was confirmed by the measurements with AFM and SEM, which even showed a discrepancy of about 31 percent. Thus, I showed in my work that sedimentation experiments offer a possibility to accurately measure particle properties like the radius or the density.
This is a strong advantage for future experiments, since it is now possible to characterize the trapped microspheres by a simple sedimentation and thus get accurate values to evaluate the outcomes of the experiments.
Further we saw that the outcomes of sedimentations directly from the wall are equivalent to those from sedimentations in the bulk. That means that it is in the future sufficient to always start the sedimentations directly at the wall, which is a major benefit since these measurements are faster to conduct and less vulnerable to disturbances.
Since this optical trap was constructed to measure in high pressure of about 1000 bar the next step should be to verify the outcomes of my work for other pressures than atmospheric pressure. I think it would be very interesting to whether the findings differ in higher pressure from those under atmospheric pressure. For performing these experiments I suggest to use the Duke Standard 9008 microspheres, since their density is well determined by the manufacturer and thus their radii will be provided by sedimentations experiments.

A. Appendix

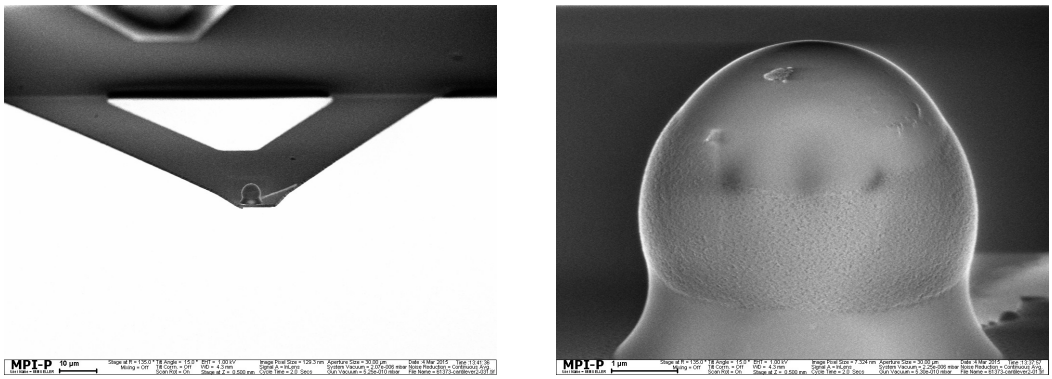

Figure A.1.: Pictures taken with an SEM of the second Bangs Laboratories, Inc. bead. Left picture shows the whole cantilever and right one a close up of the bead.
Taken by Maren Müller.

Table A.1.: Sedimentation velocities of two beads from the sample with Bangs Laboratories, Inc. microspheres with radius $r_{spec} = 2,53\ \mu m$ in water for different values of the trapping laser attenuator.

Attenuator	5 %	10 %	15 %	20 %	25 %
v_s of 1st row	$(10,38 \pm 0,05)\ \frac{\mu m}{s}$	$(9.21 \pm 0,03)\ \frac{\mu m}{s}$	$(10,14 \pm 0,03)\ \frac{\mu m}{s}$	$(10,57 \pm 0,03)\ \frac{\mu m}{s}$	$(10,10 \pm 0,02)\ \frac{\mu m}{s}$
v_s of 2nd row	$(10.20 \pm 0,02)\ \frac{\mu m}{s}$	$(10,23 \pm 0,02)\ \frac{\mu m}{s}$	$(10,91 \pm 0,03)\ \frac{\mu m}{s}$	$(10,63 \pm 0,04)\ \frac{\mu m}{s}$	$(10,00 \pm 0,04)\ \frac{\mu m}{s}$
Attenuator	30 %	35 %	40 %	45 %	50 %
v_s of 1st row	$(10,51 \pm 0,03)\ \frac{\mu m}{s}$	$(10,15 \pm 0,02)\ \frac{\mu m}{s}$	$(9.52 \pm 0,03)\ \frac{\mu m}{s}$	$(10,21 \pm 0,03)\ \frac{\mu m}{s}$	$(10,27 \pm 0,04)\ \frac{\mu m}{s}$
v_s of 2nd row	$(10,64 \pm 0,07)\ \frac{\mu m}{s}$	$(10,35 \pm 0,05)\ \frac{\mu m}{s}$	$(10,08 \pm 0,03)\ \frac{\mu m}{s}$	$(10,80 \pm 0,04)\ \frac{\mu m}{s}$	$(10,29 \pm 0,05)\ \frac{\mu m}{s}$

Table A.2.: Sedimentation velocity v_s and the resulting viscosity η^* for each sedimentation at $D = 50\mu m$, $D = 100\mu m$ and $D = 200\mu m$ as well as the mean values and standard deviations of the first sample with Duke Standard 9008 in water

Bead No. 1, $r = (3,32 \pm 0,03)\ \mu m$							
50 µm	$v_s\ [\frac{\mu m}{s}]$	33,64	33,60	35,09	33,23	33,72	Mean:
	$\eta^*\ [mPa \cdot s]$	1,11	1,11	1,06	1,12	1,10	1,10 ± 0,02
100 µm	$v_s\ [\frac{\mu m}{s}]$	35,12	34,81	34,83	35,22	34,55	Mean:
	$\eta^*\ [mPa \cdot s]$	1,06	1,07	1,07	1,06	1,08	1,07 ± 0,01
200 µm	$v_s\ [\frac{\mu m}{s}]$	36,45	35,76	36,36	37,10	36,13	Mean:
	$\eta^*\ [mPa \cdot s]$	1,02	1,04	1,02	1,00	1,03	1,02 ± 0,01
Bead No. 2, $r = (3,20 \pm 0,05)\ \mu m$							
50 µm	$v_s\ [\frac{\mu m}{s}]$	32,27	33,87	33,80	33,21	33,86	Mean
	$\eta^*\ [mPa \cdot s]$	1,08	1,03	1,03	1,05	1,03	1,04 ± 0,02
100 µm	$v_s\ [\frac{\mu m}{s}]$	34,60	34,35	34,31	35,32	35,41	Mean:
	$\eta^*\ [mPa \cdot s]$	1,01	1,01	1,02	0,99	0,98	1,00 ± 0,01
200 µm	$v_s\ [\frac{\mu m}{s}]$	35,51	34,53	35,12	34,27	35,01	Mean:
	$\eta^*\ [mPa \cdot s]$	0,98	1,01	0,99	1,02	1,00	1,00 ± 0,01
Bead No. 3, $r = (4,08 \pm 0,05)\ \mu m$							
50 µm	$v_s\ [\frac{\mu m}{s}]$	47,94	46,97	46,20	47,81	47,62	Mean:
	$\eta^*\ [mPa \cdot s]$	1,17	1,19	1,21	1,17	1,18	1,19 ± 0,02
100 µm	$v_s\ [\frac{\mu m}{s}]$	53,41	50,73	54,54	53,41	54,41	Mean:
	$\eta^*\ [mPa \cdot s]$	1,05	1,11	1,03	1,05	1,03	1,05 ± 0,03
200 µm	$v_s\ [\frac{\mu m}{s}]$	55,76	54,84	54,43	55,18	55,10	Mean:
	$\eta^*\ [mPa \cdot s]$	1,01	1,02	1,03	1,02	1,02	1,02 ± 0,01
Bead No. 4, $r = (3,76 \pm 0,03)\ \mu m$							
50 µm	$v_s[\frac{\mu m}{s}]$	40,95	41,04	43,04	42,36	41,88	Mean:
	$\eta^*\ [mPa \cdot s]$	1,17	1,17	1,11	1,13	1,15	1,15 ± 0,02
100 µm	$v_s\ [\frac{\mu m}{s}]$	47,13	47,13	46,68	47,42	47,19	Mean:
	$\eta^*\ [mPa \cdot s]$	1,02	1,02	1,03	1,01	1,02	1,02 ± 0,01
200 µm	$v_s\ [\frac{\mu m}{s}]$	49,21	48,48	47,90	48,15	48,02	Mean:
	$\eta^*\ [mPa \cdot s]$	0,97	0,99	1,00	1,00	1,00	0,99 ± 0,01

Table A.3.: Sedimentation Speed at $d = 500\ \mu m$ and resulting radius for the sample of Bangs Laboratories, Inc. microspheres with radius $r_{spec} = 2,53\ \mu m$ in water. The last column shows the mean radius with its standard deviation.

Bead No. 1	$v_s\ [\frac{\mu m}{s}]$	9,41	9,25	11,04	9,27	9,64			Mean:
	$r\ [\mu m]$	2,08	2,06	2,25	2,06	2,10			2,08 ± 0,07
Bead No. 2	$v_s\ [\frac{\mu m}{s}]$	10,89	10,96	11,25	10,75	11,12			Mean:
	$r\ [\mu m]$	2,24	2,24	2,27	2,22	2,26			2,24 ± 0,02
Bead No. 3	$v_s\ [\frac{\mu m}{s}]$	9,83	10,40	10,60	9,74	9,89			Mean:
	$r\ [\mu m]$	2,12	2,18	2,20	2,11	2,13			2,13 ± 0,04
Bead No. 4	$v_s\ [\frac{\mu m}{s}]$	10,86	9,91	10,46	10,48	9,76	10,16	9,91	Mean:
	$r\ [\mu m]$	2,23	2,13	2,19	2,19	2,12	2,16	2,13	2,16 ± 0,04

Table A.4.: Sedimentation Speed at $d = 500\ \mu m$ and resulting radius for the Bangs Laboratories, Inc. microspheres with radius $r_{spec} = 3,23\ \mu m$ in water. The last column shows the mean radius with its standard deviation.

Bead No. 1	$v_s\ [\frac{\mu m}{s}]$	15,80	15,28	15,44	15,25	16,14	Mean:
	$r\ [\mu m]$	2,69	2,65	2,66	2,64	2,72	2,66 ± 0,03
Bead No. 2	$v_s\ [\frac{\mu m}{s}]$	15,75	16,43	16,47	15,84	15,61	Mean:
	$r\ [\mu m]$	2,69	2,75	2,75	2,70	2,68	2,70 ± 0,03
Bead No. 3	$v_s\ [\frac{\mu m}{s}]$	16,04	15,59	15,25	15,85	15,31	Mean:
	$r\ [\mu m]$	2,71	2,67	2,65	2,70	2,65	2,67 ± 0,03
Bead No. 4	$v_s\ [\frac{\mu m}{s}]$	16,85	17,06	17,35	16,57	16,60	Mean:
	$r\ [\mu m]$	2,78	2,80	2,82	2,76	2,76	2,78 ± 0,02

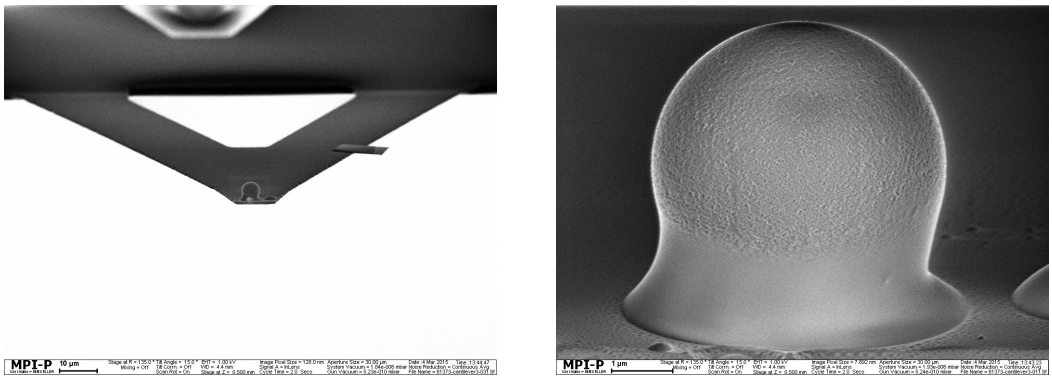

Figure A.2.: Pictures taken with an SEM of the third Bangs Laboratories, Inc. bead. Left picture shows the whole cantilever and right one a close up of the bead.
Taken by Maren Müller.

Table A.5.: Sedimentation velocity v_s and the resulting viscosity η^* for each sedimentation at $D = 50\ \mu m$, $D = 100\ \mu m$ and $D = 200\ \mu m$ as well as the mean values and standard deviations of the Bangs Laboratories, Inc. microspheres with radius $r_{spec} = 2,53\ \mu m$ in water

Bead No. 1, $r = (2,08 \pm 0,07)\ \mu m$							
50 µm	$v_s\ [\frac{\mu m}{s}]$	8,58	8,97	8,93	8,50	8,87	Mean:
	$\eta^*\ [mPa \cdot s]$	1,13	1,08	1,09	1,14	1,10	1,11 ± 0,02
100 µm	$v_s\ [\frac{\mu m}{s}]$	9,62	9,66	10,40	10,40	10,00	Mean:
	$\eta^*\ [mPa \cdot s]$	1,01	1,01	0,94	0,94	0,97	0,97 ± 0,03
200 µm	$v_s\ [\frac{\mu m}{s}]$	10,61	9,93	9,65	9,47	8,96	Mean:
	$\eta^*\ [mPa \cdot s]$	0,92	0,98	1,01	1,03	1,09	1,00 ± 0,06
Bead No. 2, $r = (2,24 \pm 0,02)\ \mu m$							
50 µm	$v_s\ [\frac{\mu m}{s}]$	9,43	9,55	9,46	9,63	9,28	Mean
	$\eta^*\ [mPa \cdot s]$	1,17	1,15	1,16	1,14	1,19	1,16 ± 0,01
100 µm	$v_s\ [\frac{\mu m}{s}]$	10,23	10,50	10,33	11,19	10,93	Mean:
	$\eta^*\ [mPa \cdot s]$	1,08	1,05	1,07	0,98	1,01	1,04 ± 0,04
200 µm	$v_s\ [\frac{\mu m}{s}]$	10,21	10,31	10,50	11,02	9,91	Mean:
	$\eta^*\ [mPa \cdot s]$	1,08	1,07	1,05	1,00	1,11	1,06 ± 0,04
Bead No. 3, $r = (2,13 \pm 0,04)\ \mu m$							
50 µm	$v_s[\frac{\mu m}{s}]$	9,09	9,75	9,23	8,98	10,19	Mean:
	$\eta^*\ [mPa \cdot s]$	1,11	1,04	1,10	1,13	0,99	1,07 ± 0,05
100 µm	$v_s\ [\frac{\mu m}{s}]$	9,20	9,77	10,05	8,84	9,44	Mean:
	$\eta^*\ [mPa \cdot s]$	1,10	1,03	1,01	1,14	1,07	1,07 ± 0,05
200 µm	$v_s\ [\frac{\mu m}{s}]$	9,72	9,85	9,39	10,53	10,11	Mean:
	$\eta^*\ [mPa \cdot s]$	1,04	1,03	1,08	0,96	1,00	1,02 ± 0,04
Bead No. 4, $r = (2,16 \pm 0,04)\ \mu m$							
50 µm	$v_s[\frac{\mu m}{s}]$	10,35	9,87	10,07	10,04	10,13	Mean:
	$\eta^*\ [mPa \cdot s]$	0,99	1,04	1,02	1,02	1,01	1,01 ± 0,02
100 µm	$v_s\ [\frac{\mu m}{s}]$	9,71	10,25	10,06	9,75	10,16	Mean:
	$\eta^*\ [mPa \cdot s]$	1,05	1,00	1,02	1,05	1,01	1,03 ± 0,02
200 µm	$v_s\ [\frac{\mu m}{s}]$	10,33	10,74	10,78	10,30	10,84	Mean:
	$\eta^*\ [mPa \cdot s]$	0,99	0,95	0,95	0,99	0,94	0,97 ± 0,02

Table A.6.: Sedimentation velocity v_s and the resulting viscosity η^* for each sedimentation at $D = 50\ \mu m$, $D = 100\ \mu m$ and $D = 200\ \mu m$ as well as the mean values and standard deviations of the Bangs Laboratories, Inc. microspheres with radius $r_{spec} = 3,23\ \mu m$ in water

Bead No. 1, $r = (2,66 \pm 0,03)\ \mu m$							
50 µm	$v_s\ [\frac{\mu m}{s}]$	14,42	13,58	13,90	12,98	13,94	Mean:
	$\eta^*\ [mPa \cdot s]$	1,08	1,15	1,12	1,20	1,12	1,14 ± 0,04
100 µm	$v_s\ [\frac{\mu m}{s}]$	14,68	14,73	14,84	14,54	14,95	Mean:
	$\eta^*\ [mPa \cdot s]$	1,06	1,06	1,05	1,07	1,04	1,06 ± 0,01
200 µm	$v_s\ [\frac{\mu m}{s}]$	15,06	15,14	15,51	16,31	16,01	Mean:
	$\eta^*\ [mPa \cdot s]$	1,04	1,03	1,01	0,96	0,98	1,00 ± 0,03
Bead No. 2, $r = (2,70 \pm 0,03)\ \mu m$							
50 µm	$v_s\ [\frac{\mu m}{s}]$	14,41	13,51	14,36	14,71	14,33	Mean
	$\eta^*\ [mPa \cdot s]$	1,11	1,19	1,12	1,17	1,12	1,14 ± 0,03
100 µm	$v_s\ [\frac{\mu m}{s}]$	15,73	14,76	15,42	15,63	15,12	Mean:
	$\eta^*\ [mPa \cdot s]$	1,02	1,09	1,04	1,03	1,06	1,05 ± 0,02
200 µm	$v_s\ [\frac{\mu m}{s}]$	15,83	15,22	15,77	15,66	15,33	Mean:
	$\eta^*\ [mPa \cdot s]$	1,01	1,03	1,02	1,02	1,05	1,03 ± 0,01
Bead No. 3, $r = (2,67 \pm 0,03)\ \mu m$							
50 µm	$v_s[\frac{\mu m}{s}]$	13,40	14,42	14,17	13,95	14,15	Mean:
	$\eta^*\ [mPa \cdot s]$	1,17	1,08	1,10	1,12	1,11	1,12 ± 0,03
100 µm	$v_s\ [\frac{\mu m}{s}]$	15,80	14,79	15,33	15,54	15,61	Mean:
	$\eta^*\ [mPa \cdot s]$	0,99	1,06	1,02	1,01	1,00	1,02 ± 0,02
200 µm	$v_s\ [\frac{\mu m}{s}]$	16,29	15,67	15,58	15,15	16,10	Mean:
	$\eta^*\ [mPa \cdot s]$	0,96	1,00	1,00	1,03	0,97	0,99 ± 0,03
Bead No. 4, $r = (2,78 \pm 0,02)\ \mu m$							
50 µm	$v_s\ [\frac{\mu m}{s}]$	14,49	14,61	14,27	14,20	13,78	Mean:
	$\eta^*\ [mPa \cdot s]$	1,17	1,16	1,19	1,19	1,23	1,19 ± 0,02
100 µm	$v_s\ [\frac{\mu m}{s}]$	15,73	16,18	16,09	15,99	14,94	Mean:
	$\eta^*\ [mPa \cdot s]$	1,08	1,05	1,05	1,06	1,13	1,07 ± 0,03
200 µm	$v_s\ [\frac{\mu m}{s}]$	16,75	16,31	15,95	16,74	16,29	Mean:
	$\eta^*\ [mPa \cdot s]$	1,01	1,04	1,06	1,01	1,04	1,03 ± 0,02

Table A.7.: Fitting parameter α at the wall and the resulting values for the viscosity η of the Bangs Laboratories, Inc. microspheres with radius $r_{spec} = 2,53\ \mu m$ in water.

Bead No. 1	$\alpha\ [10^{-6}\frac{s}{m^2}]$	-55,37	-55,43	-58,63	-58,12	-56,49	Mean:
	$\eta\ [mPa \cdot s]$	1,13	1,13	1,20	1,19	1,16	1,16 ± 0,03
Bead No. 2	$\alpha\ [10^{-6}\frac{s}{m^2}]$	-50,12	-48,61	-48,63	-46,99	-44,65	Mean:
	$\eta\ [mPa \cdot s]$	1,24	1,20	1,20	1,16	1,10	1,18 ± 0,05
Bead No. 3	$\alpha\ [10^{-6}\frac{s}{m^2}]$	-57,11	-55,63	-56,54	-55,41	-58,41	Mean:
	$\eta\ [mPa \cdot s]$	1,24	1,21	1,23	1,20	1,27	1,23 ± 0,02
Bead No. 4	$\alpha\ [10^{-6}\frac{s}{m^2}]$	-48,04	-50,57	-52,14	-53,12	-46,98	Mean:
	$\eta\ [mPa \cdot s]$	1,06	1,12	1,15	1,17	1,04	1,11 ± 0,05

Table A.8.: Fitting parameter α at the wall and the resulting values for the viscosity η of the Bangs Laboratories, Inc. microspheres with radius $r_{spec} = 3,23\ \mu m$ in water. The missing value of bead No. 2 is caused by an corrupt data file.

Bead No. 1	$\alpha\ [10^{-6}\frac{s}{m^2}]$	-26,37	-26,64	-27,17	-27,24	-26,74	Mean:
	$\eta\ [mPa \cdot s]$	1,10	1,11	1,13	1,13	1,11	1,12 ± 0,01
Bead No. 2	$\alpha\ [10^{-6}\frac{s}{m^2}]$	-	-25,23	-25,56	-25,51	-24,33	Mean:
	$\eta\ [mPa \cdot s]$	-	1,10	1,21	1,11	1,06	1,09 ± 0,02
Bead No. 3	$\alpha\ [10^{-6}\frac{s}{m^2}]$	-26,58	-24,77	-27,11	-25,88	-26,43	Mean:
	$\eta\ [mPa \cdot s]$	1,11	1,03	1,13	1,08	1,10	1,09 ± 0,03
Bead No. 4	$\alpha\ [10^{-6}\frac{s}{m^2}]$	-24,42	-25,30	-24,58	-24,48	-24,22	Mean:
	$\eta\ [mPa \cdot s]$	1,15	1,19	1,16	1,15	1,14	1,16 ± 0,02

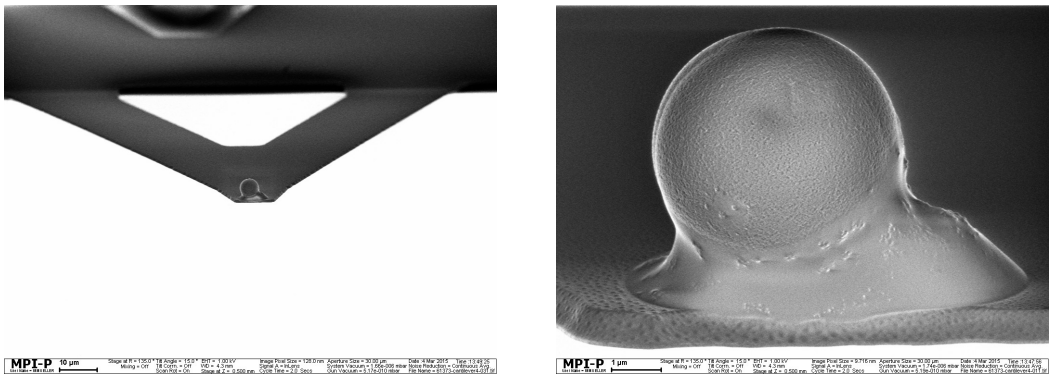

Figure A.3.: Pictures taken with an SEM of the fourth Bangs Laboratories, Inc. bead. Left picture shows the whole cantilever and right one a close up of the bead.
Taken by Maren Müller.

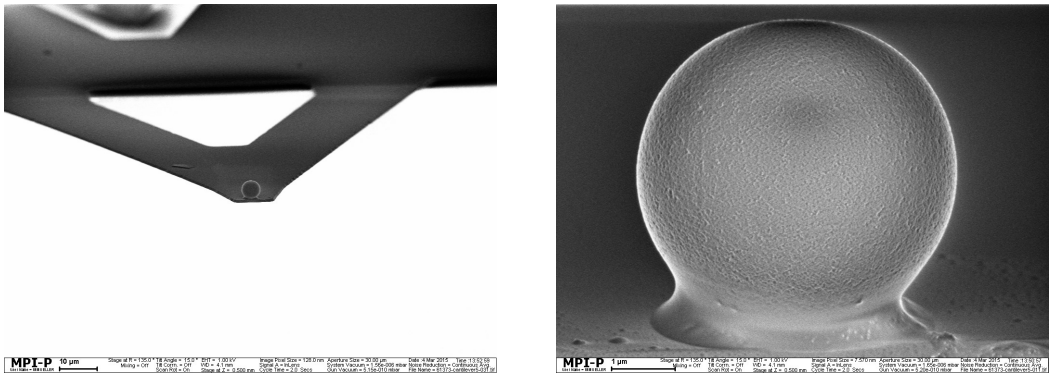

Figure A.4.: Pictures taken with an SEM of the fifth Bangs Laboratories, Inc. bead. Left picture shows the whole cantilever and right one a close up of the bead.
Taken by Maren Müller.

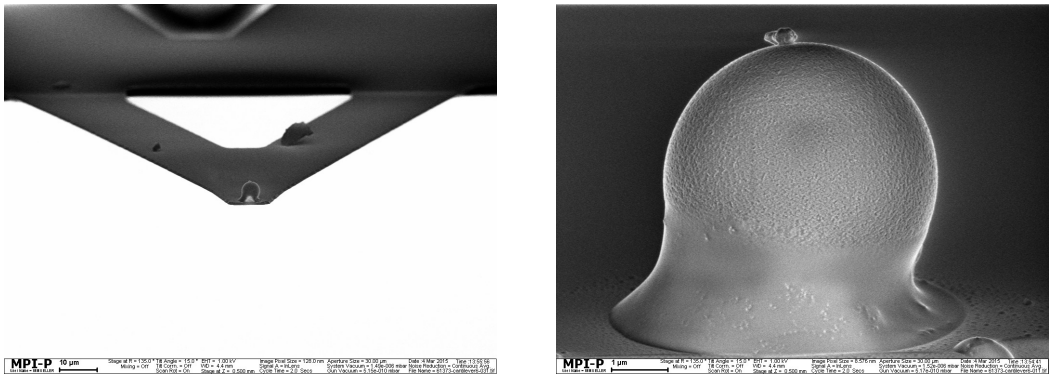

Figure A.5.: Pictures taken with an SEM of the sixth Bangs Laboratories, Inc. bead. Left picture shows the whole cantilever and right one a close up of the bead.
Taken by Maren Müller.

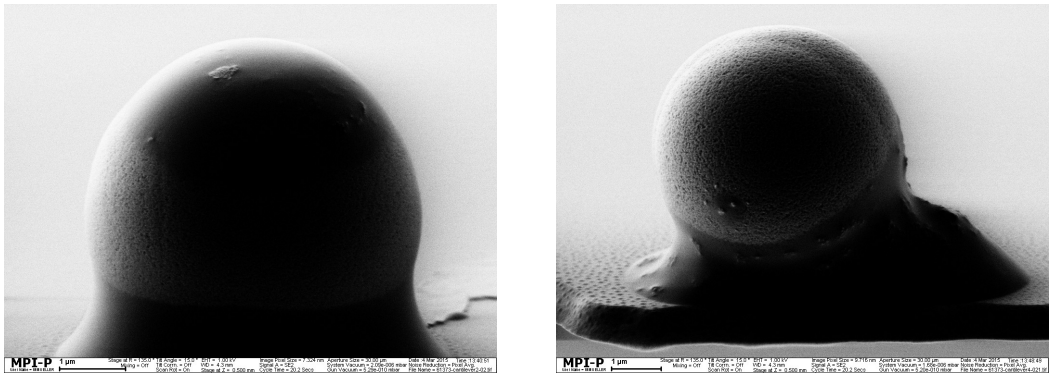

Figure A.6.: SEM picture of the second (left) and fourth (right) bead with a different filter to survey the surface structure of the microspheres.
Taken by Maren Müller

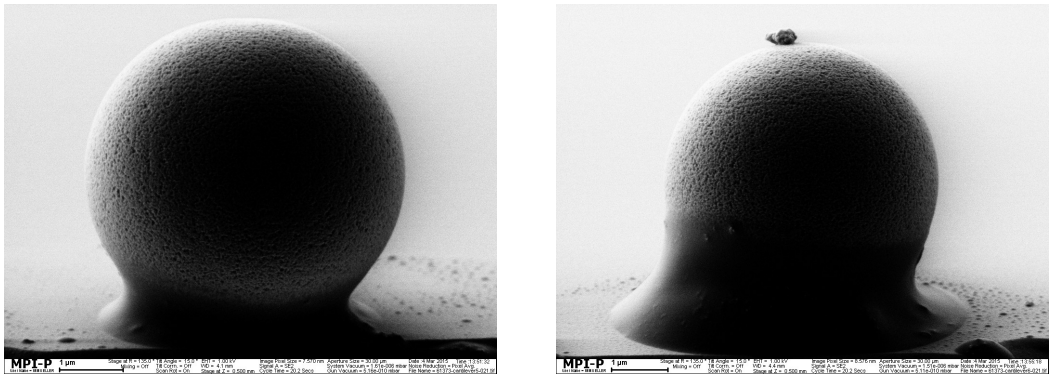

Figure A.7.: SEM picture of the fifth (left) and sixth (right) bead with a different filter to survey the surface structure of the microspheres.
Taken by Maren Müller

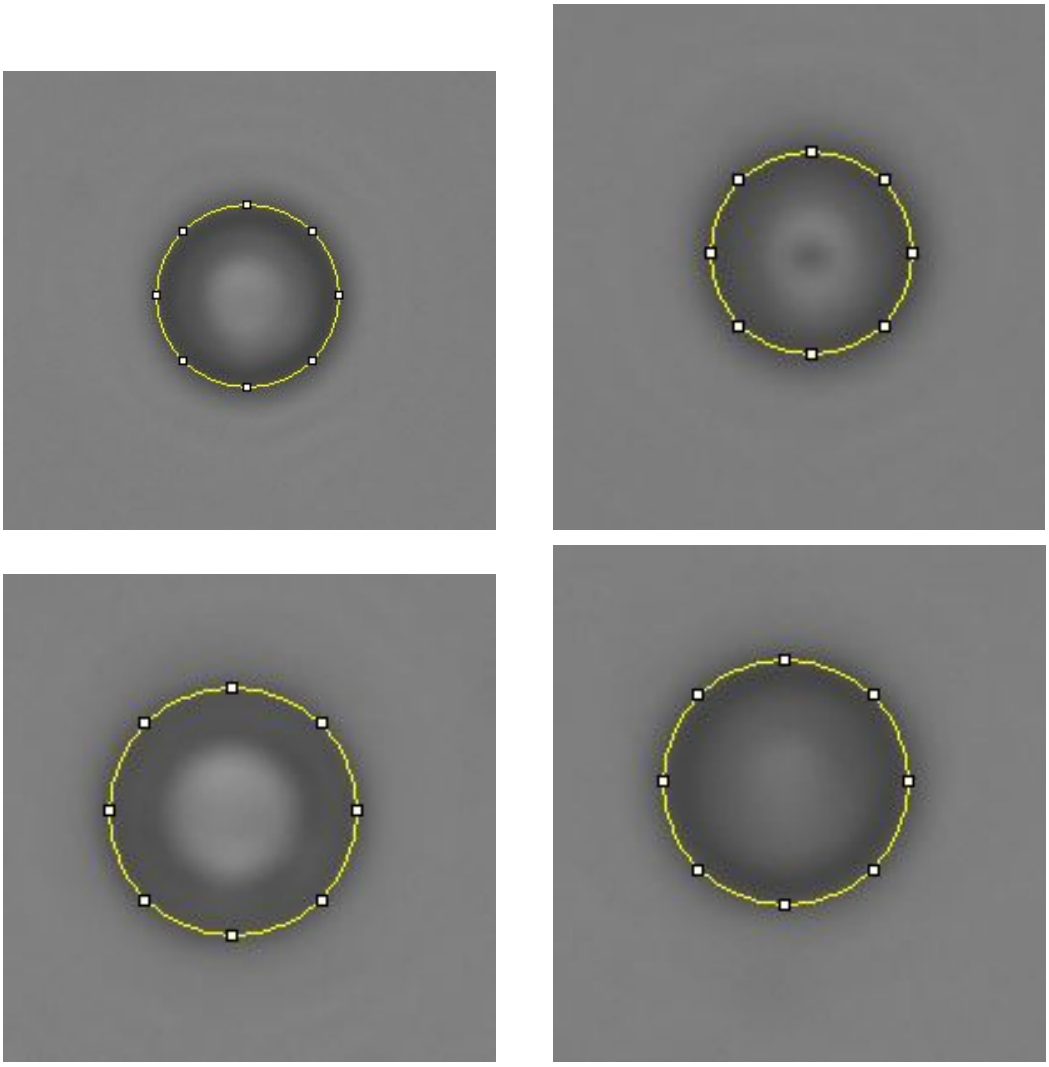

Figure A.8.: Beads of the sample with Duke Standard 9008 in 20 %vol. glycerol, processing and diameter measuring (yellow circle) with ImageJ.

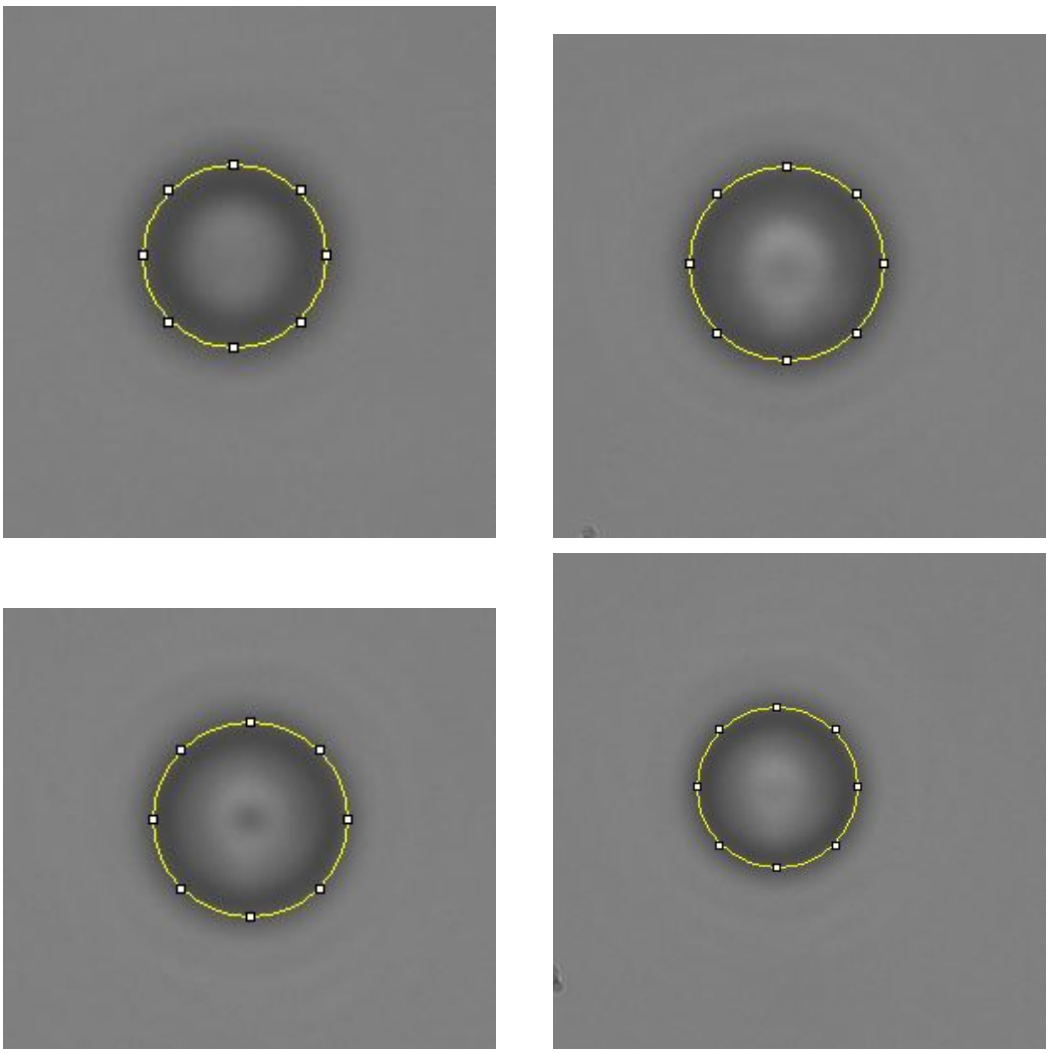

Figure A.9.: Beads of the sample with Duke Standard 9008 in 40 %vol. glycerol, processing and diameter measuring (yellow circle) with ImageJ.

Table A.9.: Sedimentation velocity v_s and the resulting viscosity η^* for each sedimentation at $D = 50\ \mu m$, $D = 100\ \mu m$, $D = 200\ \mu m$ and $D = 500\ \mu m$ as well as the mean values and standard deviations of the sample with Duke Standard 9008 in 20 %vol. glycerol.
The file of the last $D = 200\ \mu m$ sedimentation of bead No.1 was corrupt.

Bead No. 1, $r = (4,34 \pm 0,4)\ \mu m$							
50 µm	$v_s\ [\frac{\mu m}{s}]$	26,48	27,83	28,47	28,28	28,28	Mean:
	$\eta^*\ [mPa \cdot s]$	2,30	2,19	2,14	2,15	2,15	2,19 ± 0,06
100 µm	$v_s\ [\frac{\mu m}{s}]$	30,67	30,40	30,66	30,86	31,05	Mean:
	$\eta^*\ [mPa \cdot s]$	1,99	2,00	1,99	1,97	1,96	1,98 ± 0,01
200 µm	$v_s\ [\frac{\mu m}{s}]$	31,70	32,41	31,91	31,44	-	Mean:
	$\eta^*\ [mPa \cdot s]$	1,92	1,88	1,91	1,94	-	1,91 ± 0,02
500 µm	$v_s\ [\frac{\mu m}{s}]$	31,68	32,11	31,97	32,13	32,14	Mean:
	$\eta^*\ [mPa \cdot s]$	1,92	1,90	1,90	1,90	1,89	1,90 ± 0,01
Bead No. 2, $r = (3,32 \pm 0,4)\ \mu m$							
50 µm	$v_s\ [\frac{\mu m}{s}]$	18,35	18,22	18,14	18,36	18,54	Mean
	$\eta^*\ [mPa \cdot s]$	1,94	1,96	1,96	1,94	1,92	1,95 ± 0,01
100 µm	$v_s\ [\frac{\mu m}{s}]$	19,71	19,18	19,42	19,22	19,11	Mean:
	$\eta^*\ [mPa \cdot s]$	1,81	1,86	1,83	1,85	1,86	1,84 ± 0,02
200 µm	$v_s\ [\frac{\mu m}{s}]$	19,44	19,79	20,06	19,57	19,40	Mean:
	$\eta^*\ [mPa \cdot s]$	1,83	1,80	1,78	1,82	1,84	1,81 ± 0,02
500 µm	$v_s\ [\frac{\mu m}{s}]$	20,27	20,61	19,97	19,94	20,06	Mean:
	$\eta^*\ [mPa \cdot s]$	1,76	1,73	1,78	1,79	1,78	1,77 ± 0,02
Bead No. 3, $r = (4,11 \pm 0,4)\ \mu m$							
50 µm	$v_s\ [\frac{\mu m}{s}]$	16,78	17,53	17,41	17,09	17,82	Mean:
	$\eta^*\ [mPa \cdot s]$	3,25	3,12	3,14	3,20	3,06	3,15 ± 0,07
100 µm	$v_s\ [\frac{\mu m}{s}]$	25,10	26,85	26,83	27,23	27,22	Mean:
	$\eta^*\ [mPa \cdot s]$	2,18	2,03	2,04	2,01	2,01	2,05 ± 0,06
200 µm	$v_s\ [\frac{\mu m}{s}]$	26,10	26,98	56,26	25,26	26,30	Mean:
	$\eta^*\ [mPa \cdot s]$	2,09	2,02	2,16	2,16	2,08	2,10 ± 0,05
500 µm	$v_s\ [\frac{\mu m}{s}]$	26,01	25,34	25,61	25,52	25,87	Mean:
	$\eta^*\ [mPa \cdot s]$	2,10	2,16	2,13	2,14	2,11	2,13 ± 0,02
Bead No. 4, $r = (4,11 \pm 0,4)\ \mu m$							
50 µm	$v_s\ [\frac{\mu m}{s}]$	28,39	28,14	27,73	28,41	27,77	Mean:
	$\eta^*\ [mPa \cdot s]$	1,92	1,94	1,97	1,92	1,97	1,94 ± 0,02
100 µm	$v_s\ [\frac{\mu m}{s}]$	29,72	29,62	29,90	29,75	29,69	Mean:
	$\eta^*\ [mPa \cdot s]$	1,84	1,84	1,83	1,84	1,84	1,84 ± 0,01
200 µm	$v_s\ [\frac{\mu m}{s}]$	29,69	29,62	29,64	30,25	29,73	Mean:
	$\eta^*\ [mPa \cdot s]$	1,84	1,84	1,84	1,81	1,84	1,83 ± 0,01
500 µm	$v_s\ [\frac{\mu m}{s}]$	30,76	31,02	30,06	29,81	30,06	Mean:
	$\eta^*\ [mPa \cdot s]$	1,78	1,76	1,82	1,83	1,83	1,80 ± 0,03

Table A.10.: Sedimentation velocity v_s and the resulting viscosity η^* for each sedimentation at $D = 50\ \mu m$, $D = 100\ \mu m$, $D = 200\ \mu m$ and $D = 500\ \mu m$ as well as the mean values and standard deviations of the sample with Duke Standard 9008 in 40 %vol. glycerol

Bead No. 1, $r = (3,61 \pm 0,4)\ \mu m$							
50 µm	$v_s\ [\frac{\mu m}{s}]$	10,79	10,27	10,35	10,48	10,46	Mean:
	$\eta^*\ [mPa \cdot s]$	3,73	3,92	3,89	3,84	3,85	3,85 ± 0,06
100 µm	$v_s\ [\frac{\mu m}{s}]$	10,85	10,86	10,78	10,58	10,77	Mean:
	$\eta^*\ [mPa \cdot s]$	3,71	3,71	3,74	3,81	3,74	3,74 ± 0,04
200 µm	$v_s\ [\frac{\mu m}{s}]$	11,38	10,97	10,97	10,99	11,01	Mean:
	$\eta^*\ [mPa \cdot s]$	3,54	3,67	3,67	3,67	3,66	3,64 ± 0,05
500 µm	$v_s\ [\frac{\mu m}{s}]$	11,04	11,09	11,29	11,09	11,14	Mean:
	$\eta^*\ [mPa \cdot s]$	3,65	3,63	3,57	3,63	3,62	3,62 ± 0,03
Bead No. 2, $r = (4,15 \pm 0,4)\ \mu m$							
50 µm	$v_s\ [\frac{\mu m}{s}]$	12,74	12,63	12,85	12,79	12,94	Mean
	$\eta^*\ [mPa \cdot s]$	4,18	4,21	4,14	4,16	4,11	4,16 ± 0,04
100 µm	$v_s\ [\frac{\mu m}{s}]$	13,65	13,61	13,85	13,79	13,81	Mean:
	$\eta^*\ [mPa \cdot s]$	3,90	3,91	3,84	3,86	3,86	3,87 ± 0,03
200 µm	$v_s\ [\frac{\mu m}{s}]$	14,15	14,52	14,39	14,07	14,03	Mean:
	$\eta^*\ [mPa \cdot s]$	3,76	3,67	3,70	3,79	3,80	3,74 ± 0,05
500 µm	$v_s\ [\frac{\mu m}{s}]$	14,08	14,39	14,38	14,22	14,59	Mean:
	$\eta^*\ [mPa \cdot s]$	3,78	3,70	3,70	3,75	3,65	3,72 ± 0,05
Bead No. 3, $r = (4,07 \pm 0,4)\ \mu m$							
50 µm	$v_s\ [\frac{\mu m}{s}]$	11,35	10,65	10,92	10,98	10,86	Mean:
	$\eta^*\ [mPa \cdot s]$	4,51	4,81	4,69	4,66	4,71	4,68 ± 0,10
100 µm	$v_s\ [\frac{\mu m}{s}]$	12,96	12,85	12,73	12,56	12,78	Mean:
	$\eta^*\ [mPa \cdot s]$	3,95	3,98	4,02	4,08	4,01	4,01 ± 0,04
200 µm	$v_s\ [\frac{\mu m}{s}]$	13,11	12,88	13,02	13,20	13,09	Mean:
	$\eta^*\ [mPa \cdot s]$	3,90	3,98	3,93	3,88	3,91	3,92 ± 0,03
500 µm	$v_s\ [\frac{\mu m}{s}]$	12,90	13,13	13,10	13,08	13,04	Mean:
	$\eta^*\ [mPa \cdot s]$	3,97	3,90	3,91	3,91	3,93	3,92 ± 0,02
Bead No. 4, $r = (3,94 \pm 0,4)\ \mu m$							
50 µm	$v_s\ [\frac{\mu m}{s}]$	11,91	11,97	12,10	11,78	12,14	Mean:
	$\eta^*\ [mPa \cdot s]$	4,03	4,01	3097	4,07	3,95	4,01 ± 0,04
100 µm	$v_s\ [\frac{\mu m}{s}]$	12,77	12,97	12,83	12,70	12,85	Mean:
	$\eta^*\ [mPa \cdot s]$	3,76	3,70	3,74	3,78	3,74	3,74 ± 0,03
200 µm	$v_s\ [\frac{\mu m}{s}]$	13,25	12,78	12,98	13,12	13,07	Mean:
	$\eta^*\ [mPa \cdot s]$	3,62	3,76	3,70	3,66	3,67	3,72 ± 0,04
500 µm	$v_s\ [\frac{\mu m}{s}]$	12,84	12,70	12,94	13,00	13,11	Mean:
	$\eta^*\ [mPa \cdot s]$	3,74	3,78	3,71	3,69	3,66	3,72 ± 0,04

Table A.11.: Comparison of mean values of viscosities η^* for the sample with Duke Standard 9008 in 40 %vol. glycerol to expectations for the Brenner factor.

D in μm	50	100	200	500
$\bar{\eta}^*$ in $mPa \cdot s$	$4,17 \pm 0,32$	$3,84 \pm 0,12$	$3,75 \pm 0,12$	$3,74 \pm 0,12$
η^*_{lit} in $mPa \cdot s$	$5,21 \pm 0,02$	$5,02 \pm 0,01$	$4,93 \pm 0,01$	$4,87 \pm 0,01$
Deviation in %	-20	-24	-24	-23

Table A.12.: Fitting parameter α at the wall and the resulting values for the viscosity η of the sample with Duke Standard 9008 in 40 %vol. glycerol.

Bead No. 1	α $[10^{-6}\frac{s}{m^2}]$	-25,37	-25,69	-25,16	-25,84	-25,75	Mean:
	η $[mPa \cdot s]$	3,69	3,74	3,66	3,76	3,74	3,72 ± 0,04
Bead No. 2	α $[10^{-6}\frac{s}{m^2}]$	-17,14	-17,36	-17,43	-17,51	-17,72	Mean:
	η $[mPa \cdot s]$	3,79	3,84	3,85	3,87	3,92	3,85 ± 0,04
Bead No. 3	α $[10^{-6}\frac{s}{m^2}]$	-19,10	-19,20	-18,91	-18,71	-19,17	Mean:
	η $[mPa \cdot s]$	3,98	4,00	3,94	3,90	4,00	3,96 ± 0,04
Bead No. 4	α $[10^{-6}\frac{s}{m^2}]$	-19,89	-20,02	-19,82	-20,29	-19,88	Mean:
	η $[mPa \cdot s]$	3,76	3,79	3,75	3,84	3,76	3,78 ± 0,03

B. Literature

Bibliography

[1] A. Ashkin, "Acceleration and Trapping of Particles by Radiation Pressure," Physical Review Letters 24, 156 (1970).

[2] H. G. O. Becker, W. Berger, G. Domschke, "Organikum - Organisch-chemisches Grundpraktikum," 16. Auflage, Deutscher Verlag der Wissenschaften Berlin, 648 (1986).

[3] H.-J. Butt, M. Kappl, "Surface and Interfacial Forces," Wiley-VCH, Weinheim (2012).

[4] Calculate density and viscosity of glycerol/water mixtures, Retrieved from `http://www.met.reading.ac.uk/~sws04cdw/viscosity_calc.html`, (18th of June, 2015).

[5] CHEMIE.DE, "Glycerin," Retrieved from `http://www.chemie.de/lexikon/Glycerin.html`, (21st of June, 2015).

[6] N. S. Cheng, "Formula for viscosity of glycerol-water mixture," Industrial and Engineering Chemistry Research 47, 3285-3288 (2008)

[7] J. P. Cleveland, S. Manne, D. Bocek, P. K. Hansma, "A nondestructive method for determining the spring constant of cantilevers for scanning force microscopy," Review of Scientific Instruments 64, 403 (1993).

[8] CVI Melles Griot, "Gaussian Beam Optics."

[9] ImageJ, `http://imagej.nih.gov/ij/`, (14th of June, 2015).

[10] M. Kehr, "Aufbau eines Hochtemperaturviskosimeters und Messung der Viskosität von Schmelzen des Systems Aluminium-Nickel," `http://nbn-resolving.de/urn/resolver.pl?urn=urn:nbn:de:bsz:ch1-200901755`, (9th of June, 2015).

[11] LabVIEW, `http://www.ni.com/labview/d/`, (18th of June, 2015).

[12] L. Limozin, K. Sengupta, "Quantitative Reflection Interference Contrast Microscopy (RICM) in Soft Matter and Cell Adhesion," ChemPhysChem 10, 2752 – 2768 (2009).

[13] J. E. Molloy, M. J. Padgett, "Lights, action: optical tweezer," Contemporary Physics 43, 241-258 (2002).

[14] K. C. Neumann, S. M. Block, "Optical trapping," Rev. Sci. Instrum. 75, 2787 (2004).

[15] S. A. Self, "Focusing of spherical Gaussian beams," Applied Optics Vol. 22 No. 5, 658-661 (1993).

[16] Uni Magdeburg, "Stoffwerte-Flüssigkeiten," Retrieved from `http://www.uni-magdeburg.de/isut/LSS/Lehre/Arbeitsheft/IV.pdf`, (11th of June, 2015).

C. Acknowledgement

I want to thank Prof. Dr. Hans-Jürgen Butt that he offered me the possibility to perform my bachelor thesis at the MPIP. Furthermore I want to thank Prof. Dr. Thomas Palberg for agreeing to correct and evaluate my thesis.
Big thanks go to Dominik Pilat for showing me how to work with the optical trap, for being relentless in giving me advices on my thesis and never growing tired of my many questions.
I thank Maren Müller and Dr. Michael Kappl for conducting the measurements on AFM and SEM, explaining the principles of these techniques to me and giving me further advice on my evaluation.
Furthermore I want to thank Dr. Rüdiger Berger, Dr. Günter Auernhammer, Thomas Nick and everybody who took part in the small group meetings for helping me in word and deed.
Lust but not least I want to thank Matthew Grafton for reading my thesis carefully and checking for any grammar and spelling mistakes.